AD

TECHNICAL REPORT

75-101-AMEL

MEASUREMENT OF WIND LOADS ON LARGE-SCALE AIR-SUPPORTED SHELTERS

Bolt, Beranek & Newman, Inc.
Cambridge, Massachusetts 02138

Contract No. DAAG17-73-C-0264

Approved for public release;
distribution unlimited.

May 1975

UNITED STATES ARMY
NATICK DEVELOPMENT CENTER
NATICK, MASSACHUSETTS 01760

Aero Mechanical Engineering
Laboratory

Approved for public release; distribution unlimited.

Citation of trade names in this report does not constitute an official indorsement or approval of the use of such items.

Destroy this report when no longer needed. Do not return it to the originator.

Unclassified

SECURITY CLASSIFICATION OF THIS PAGE *(When Data Entered)*

REPORT DOCUMENTATION PAGE		READ INSTRUCTIONS BEFORE COMPLETING FORM
1. REPORT NUMBER Technical Report 75-101-AMEL	2. GOVT ACCESSION NO.	3. RECIPIENT'S CATALOG NUMBER
4. TITLE *(and Subtitle)* MEASUREMENT OF WIND LOADS ON LARGE-SCALE AIR-SUPPORTED SHELTERS		5. TYPE OF REPORT & PERIOD COVERED 6. PERFORMING ORG. REPORT NUMBER
7. AUTHOR*(s)* Richard Madden, Hugh A. Wright, Bruce E. Murray, Anthony R. Clemente, James D. Blackwell		8. CONTRACT OR GRANT NUMBER*(s)* DAAG17-73-C-0264
9. PERFORMING ORGANIZATION NAME AND ADDRESS Bolt Beranek and Newman Inc. 50 Moulton St. Cambridge, MA 02138		10. PROGRAM ELEMENT, PROJECT, TASK AREA & WORK UNIT NUMBERS 6.27.23.A 1T762723AH98 AE 001BG
11. CONTROLLING OFFICE NAME AND ADDRESS US Army Natick Development Center Aero-Mechanical Engineering Laboratory Natick, MA 01760		12. REPORT DATE May 1975 13. NUMBER OF PAGES 55
14. MONITORING AGENCY NAME & ADDRESS*(if different from Controlling Office)*		15. SECURITY CLASS. *(of this report)* Unclassified 15a. DECLASSIFICATION/DOWNGRADING SCHEDULE

16. DISTRIBUTION STATEMENT *(of this Report)*

Approved for public release; distribution unlimited.

17. DISTRIBUTION STATEMENT *(of the abstract entered in Block 20, if different from Report)*

18. SUPPLEMENTARY NOTES

19. KEY WORDS *(Continue on reverse side if necessary and identify by block number)*

SHELTERS	TENTS	WIND TUNNEL TESTS
AIR SUPPORTED SHELTERS	TENTAGE	WIND VELOCITY
LOADS (FORCES)	CLOTHING	PRESSURE
WIND LOADS	EQUIPMENT	TESTS
INFLATABLE STRUCTURES	PACKAGING TECHNOLOGY	MEASUREMENTS

20. ABSTRACT *(Continue on reverse side if necessary and identify by block number)*

Wind tunnel tests on a double-wall and a single-wall air-supported shelter are described. Included is a description of the test facility, test items and instrumentation. The procedures used for data acquisition and reduction are discussed. Results are presented in terms of aerodynamic load coefficients, pressure distribution, anchor loads and spectra of the shelter acceleration and anchor loads. These results are compared with previous

DD FORM 1 JAN 73 1473 EDITION OF 1 NOV 65 IS OBSOLETE

SECURITY CLASSIFICATION OF THIS PAGE *(When Data Entered)*

20. ABSTRACT (Cont-d)

results obtained using models of air-supported shelters and with some rigid structure results. The results show that the previous model results underestimate the anchor load by a factor of 2, and a new procedure for the design of anchor loads is suggested. The aerodynamic loads are in reasonable agreement with the model results, and the pressure distributions are typical of those found experimentally for rough cylinders.

PREFACE

This report written by Bolt, Beranek and Newman, Inc. under contract DAAG17-73-C-0264 culminates an effort to verify design data for air-supported shelters obtained with scale models. The results presented for wind-loading of full-scale shelters will be used in future designs of air-supported shelters. The work was carried out under the task, "Studies in the Mechanics of Tentage Materials and Structures" within the Clothing, Equipment and Packaging Technology project. Jack M. Siegel of the Aero-Mechanical Engineering Laboratory, Natick Development Center was the project officer for this program with Earl C. Steeves and Arthur L. Murphy participating as primary members of the task team. Appreciation is expressed to William L. Crenshaw, Arthur R. Johnson, and Ernest E. Saab for their assistance during the entire course of this program and especially during the set-up for the conduct of the wind tunnel tests.

TABLE OF CONTENTS

	page
LIST OF FIGURES	v
SUMMARY	vii
1. INTRODUCTION	1
2. DESCRIPTION OF TEST FACILITY, TEST ITEMS, AND INSTRUMENTATION	3
2.1 Test Facility	3
2.2 Ground Plane	3
2.3 Shelter Descriptions	3
2.4 Instrumentation	5
2.4.1 Tie-down loads	5
2.4.2 Pressure distribution	14
2.4.3 Acceleration	14
3. DATA ACQUISITION AND REDUCTION	15
3.1 Data Acquisition	15
3.2 Data Reduction	15
4. SUMMARY OF TEST CONDITIONS	17
5. RESULTS AND DISCUSSION	20
5.1 Double-Wall Shelter	20
5.1.1 Loads	20
5.1.2 Pressure distributions	32
5.1.3 Spectra of tie-down loads and shelter accelerations	32
5.2 Single-Wall Shelter	35
5.2.1 Inflation loads	35
5.2.2 Aerodynamic loads	42

TABLE OF CONTENTS *(Cont'd.)*

page

5.2.3 Pressure distribution 45

5.2.4 Spectra of tie-down loads and shelter accelerations 45

6. COMPARISON OF LARGE-SCALE SHELTER ANCHOR LOADS WITH EXTRAPOLATED RESULTS FROM SCALE MODELS 50

6.1 Double-Wall Shelter 50

6.2 Single-Wall Shelter 51

REFERENCES 53

LIST OF SYMBOLS 54

DD FORM .....

LIST OF FIGURES

Figure		page
1.	Double Wall Shelter Mounted on Ground Plane ...	4
2.	Location of Force Transducers on Double-Wall Shelter	6
3.	Location of Uninstrumented End-Wall Tie-Downs (0° Orientation)	7
4a.	Location of Pressure Taps on Sides of Double-Wall Shelter	8
4b.	Location of Pressure Taps on End Walls of Double-Wall Shelter	9
5.	Single-Wall Shelter Mounted on Ground Plane ...	10
6.	Location of Four Transducers on Single-Wall Shelter	11
7.	Location of Pressure Taps on Single-Wall Shelter	12
8.	Three Component Load Transducer With Cover Removed	13
9.	Data Acquisition System	16
10.	Lift and Drag Coefficient as a Function of Reynolds Number	21
11.	Comparison of Anchor Loads With and Without End-Wall Grommets Attached to Ground Plane	23
12.	Summary of Force Coefficients at q = 30 as a Function of Orientation	24
13.	Anchor and Guyline Coefficients as a Function of Reynolds Number	26
14a.	Distribution of Guyline and Anchor Load at $\theta = 0°$	28
14b.	Distribution of Anchor and Guyline Load at $\theta = \pi/4$	29

LIST OF FIGURES *(Cont'd.)*

Figure		page
14c.	Distribution of Anchor and Guyline Load at $\theta = \pi/2$	30
15.	Summary of Maximum Anchor and Guyline Load	31
16.	Pressure Distribution on Double-Wall Shelter as a Function of Angle at 0° Orientation	33
17.	Nondimensional Pressure Distribution on Shelter End Wall at an Orientation of 90°	34
18.	Comparison of the Anchor Load and Fabric Acceleration Spectra for Test 3	36
19.	Vertical Inflation Load as a Function of Internal Pressure	37
20.	Inflation Load Distribution	39
21.	Planform Area Distribution for Loading Profile.	40
22.	Summary of Inflation Loads	41
23.	Lift and Drag Coefficient as a Function of Reynolds Number	43
24.	Summary of Force Coefficients as a Function of Orientation	44
25.	Summary of Anchor Coefficients as a Function of Reynolds Number for the Single-Wall Shelter at the $\pi/4$ Orientation	46
26.	Aerodynamic and Inflation Load Distribution for the Single-Wall Shelter at the $\pi/4$ Orientation.	47
27.	Pressure Distribution on Single-Wall Shelter as a Function of Angle at 0 Orientation	48

SUMMARY

A testing program was conducted to determine the tie-down loadings that occur on large-scale single- and double-wall inflatable shelters when they are subjected to high winds. The program confirmed some previous results, gave considerable additional insight into the response of shelters, and pointed out areas where additional research is required.

In general, for the range of internal pressures and wind velocities tested, both shelters were remarkably stable, although the double-wall shelter exhibited some fluctuations in the anchor and guyline loads at high wind speeds. The frequency band of interest for these tests was 0 to 10 Hz. For the double-wall shelter, the maximum ratio of standard deviation to mean of the tie-down loads was on the order of 0.2. For the single-wall shelter, there were virtually no fluctuations in the load, and the ratio of standard deviations to mean rarely exceeded 0.05.

The use of aerodynamic coefficients, such as lift and drag, was not found to be particularly relevant in determining the tie-down loads; e.g., some of the drag force was reacting by friction between the shelter floor and the ground plane, and the lift coefficient did not account for the increment in pressurization that resulted from the static pressure drop when the tunnel was operating.

Certain comments can be made about each type of shelter.

Double-Wall Shelter

1. For the configuration tested, the peak anchor and guyline loads were approximately equal.

2. Loadings on the tie-downs for the sides of the shelter were much greater than those for the end-wall tie-downs, regardless of orientation.

3. Unusually high vertical forces were measured when the end walls were not securely fastened to the ground plane and when air was allowed to flow and stagnate under the shelter floor.

Single-Wall Shelter

1. The inflation pressure load distribution was not uniform for equally spaced tie-downs.

2. The aerodynamic load distribution was similar in shape to the inflation pressure distribution for the conditions tested.

3. Total inflation pressure load was proportional to the area of shelter floor that contacted the ground plane, not the planform area.

4. Differences in initial tension of tie-downs appeared to account for a variation of approximately 20% in tie-down loads over that expected.

These comments and other material, discussed fully in the text, lead us to recommend consideration of the following areas for additional research on inflatable shelters:

- A program should be conducted to determine the variation in loadings that result from variations in rigging of the shelter.
- Additional double-wall testing should be conducted to ascertain the loads that occur on the uninstrumented tie-downs and to evaluate the effects of air stagnating beneath the shelter floor.
- Additional orientations should be tested to assure that we have determined the maximum loading conditions for both single- and double-wall shelters.

1. INTRODUCTION

Air-supported shelters for temporary and permanent edifices have recently interested both military and civilian groups. A major requirement, particularly in military applications, is that these structures will be able to survive conditions of high wind loading over extended periods. Unfortunately, the response of flexible shelters to wind loadings is difficult to determine analytically; and, therefore, previous estimates of their ability to survive were obtained only from in-service experience and wind tunnel model tests. Testing of these shelters to assure that they will survive can be conducted either in the field or in a suitable wind tunnel. Testing in the field is obviously attractive because it accommodates large structures; however, wind conditions in the field are unreliable, and instrumentation of the shelter and associated data taking are practical impossibilities. Wind tunnel testing, on the other hand, offers the advantages of both controlled, reliable wind conditions and relatively easy instrumentation and data collection. However, models in wind tunnels are usually restricted in size, and scaling laws must be postulated to extrapolate results to full-size structures. In fact, a number of previous wind tunnel studies have been conducted on model shelters [1,2], and postulated scaling principles have been used to extrapolate these results to large-scale structures. The results of these studies have also been used to create a design manual [3], which the shelter designer may use to determine anchor and guyline loadings for a particular wind condition. Clearly, the costs involved in constructing and assembling a large-scale air-supported shelter, not to mention the costs associated with failure of a shelter design, require that estimates of wind loadings be accurate. The designer may, however, be uneasy when he realizes that the data he uses to evaluate wind loadings were extrapolated over perhaps two orders of magnitude in the size-scaling parameter. In recognition of this problem, the present testing program was conducted on the largest possible model shelters in the largest available wind tunnel, both to obtain additional data on wind loadings and to gain confidence in currently used extrapolation prodecures.

The present test program consisted of 57 tests, made at various wind speeds, internal pressures, and shelter orientations on models of both single-wall and double-wall shelters. In addition to the usual tunnel monitoring instrumentation, each shelter was instrumented with three-directional force transducers [4] at tie-down points, an array of pressure ports to determine surface pressure, and an accelerometer

to evaluate vibration. Each test was photographed with both still and motion picture cameras.

This report presents a summary of the test program, together with a discussion of the results obtained and a comparison of these results with those obtained in previous programs.

2. DESCRIPTION OF TEST FACILITY, TEST ITEMS, AND INSTRUMENTATION

2.1 Test Facility

Tests were conducted in the NASA Ames Research Center 40 ft × 80 ft Wind Tunnel, located at Moffett Field, California.* This wind tunnel, the largest in the United States, was chosen to permit testing of the largest possible shelter models.

The tunnel has a closed test section with semicircular sides and closed-circuit air return passage. The facility is powered by six electric motors and is capable of wind speeds up to about 0.9 km/sec.

2.2 Ground Plane

A ground plane was mounted off the tunnel floor to raise the shelters above the wind tunnel boundary layer. The ground plane was octagonal in shape and measured 12.2 m between parallel sides. The plane was of sandwich construction, approximately 12.7 cm thick, with a paper honeycomb bounded by plywood sheets. The edges of the plane were fitted with an aluminum fairing to optimize the aerodynamic configuration. The ground plane was mounted to wide flange section, which raised it to approximately 0.61 m above the tunnel floor. Figure 1 is a photograph of the ground plane with the double-wall shelter mounted on it. A similar ground plane was used for the single-wall shelter.

2.3 Shelter Descriptions

Two models of air-supported shelters were tested. The first (Fig. 1) was of double-wall construction; structural rigidity in this type of shelter is achieved by the stiffness resulting from pressure inside the two layers. The material used in fabricating the shelter was vinyl-coated nylon. The shelter was approximately 6.1 m square × 3 m high and was constructed from two separate sections, joined at the center. The shelter was attached to the ground plane at 12 anchor positions located at the periphery of the shelter and at 12 guyline positions attached at positions 6/10 of the height

---

*Throughout this report, the International System of Units (SI) has been used. However, the customary title of the NASA Ames tunnel, as well as its measurement, is the 40 ft × 80 ft Wind tunnel.

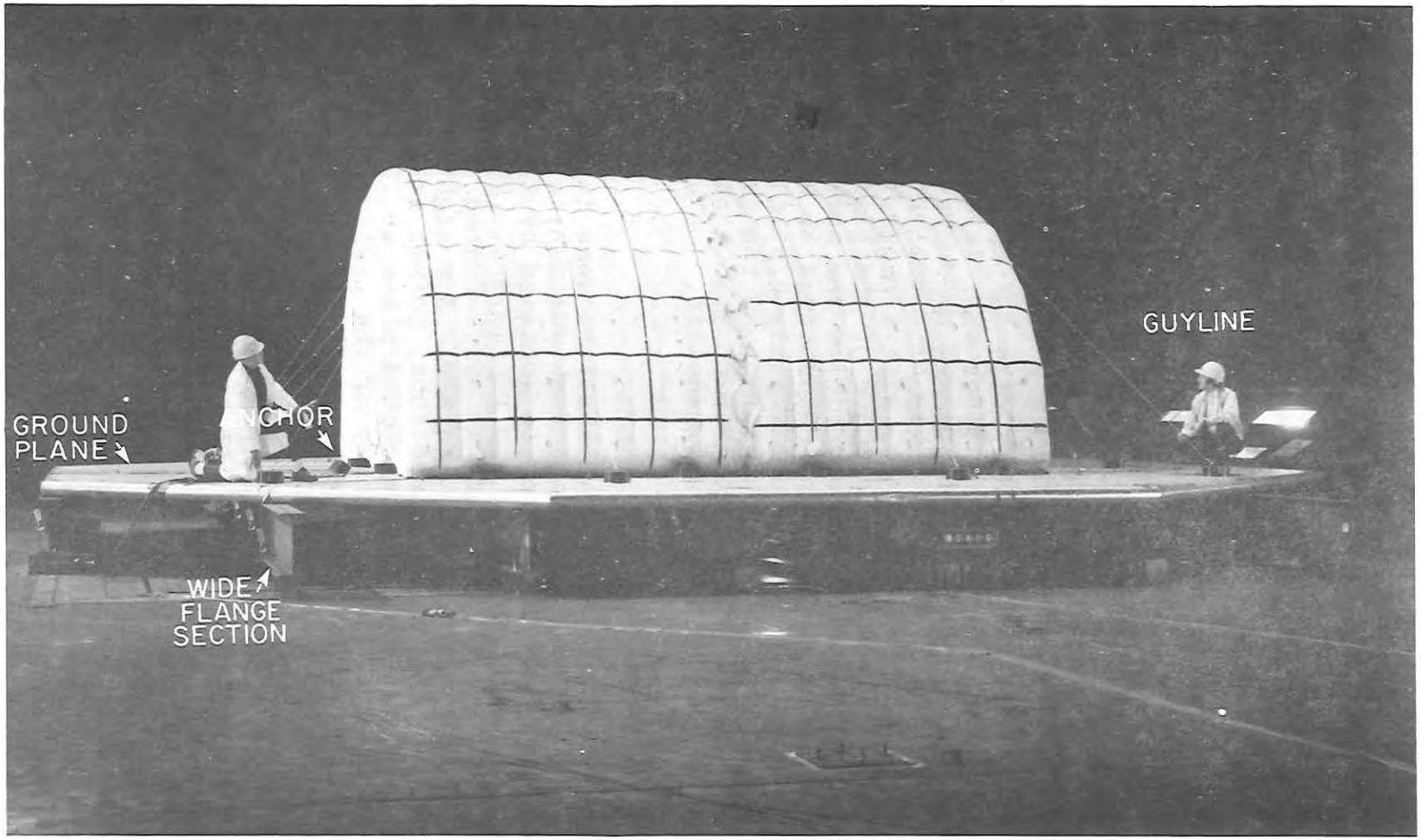

FIG. 1. DOUBLE-WALL SHELTER MOUNTED ON GROUND PLANE. [PHOTO COURTESY OF NASA AMES RESEARCH CENTER.]

from the ground. Locations of these tie-downs plus appropriate dimensional data are given in Fig. 2. In addition, the double-wall shelter had six uninstrumented tie-downs at each end curtain that were bolted to the ground plane. Locations of these tie-downs are shown in Fig. 3; they were bolted to the platform in order to eliminate air flow under the shelter floor, since air flow might have affected the lift readings adversely.* Loads at these tie-downs were not measured, and therefore total quantities, such as lift and drag, can be expected to be underestimated by some amount. Estimates of that amount will be given in a later section. The shelter also had 86 pressure taps on its surface (see Figs. 4a and 4b) for use in estimating the static pressure distribution.

The second shelter (Fig. 5) was of single-wall construction. A single-wall shelter relies upon internal pressure sustained by an air lock for its structural rigidity. This shelter was also composed of vinyl-coated nylon and was approximately 11 m long × 5.5 m in diameter and 2.1 m high. The shelter was attached to the ground plane at 26 anchor positions located at the periphery of the shelter. Locations of these tie-downs and appropriate dimensional data are given in Fig. 6. As shown in Fig. 7, the single-wall shelter has 70 pressure taps on its surface.

2.4 Instrumentation

2.4.1 Tie-down loads

Tie-down loads data were measured using three-component load sensors especially constructed for this testing program. A brief description of these load sensors follows; a more detailed description is given in Ref. 4. The transducer (Fig. 8) is a strain-gauge load sensor that has active elements for making measurements in three perpendicular directions. It is equipped with a swivel at the load introduction point to allow it to align itself with the instantaneous direction of the tie-down cable without introducing spurious loads or moments. The rated load on the transducer is 8.96 kN (linear output is, however, obtained to up to approximately 15 kN); its crosstalk in any given direction is less than 1%; and it is insensitive to thermal changes and wind loadings. On-site calibration was provided by using an insert resistor to unbalance the bridge.

---

*The effectiveness of this bolting procedure will be discussed in a following section.

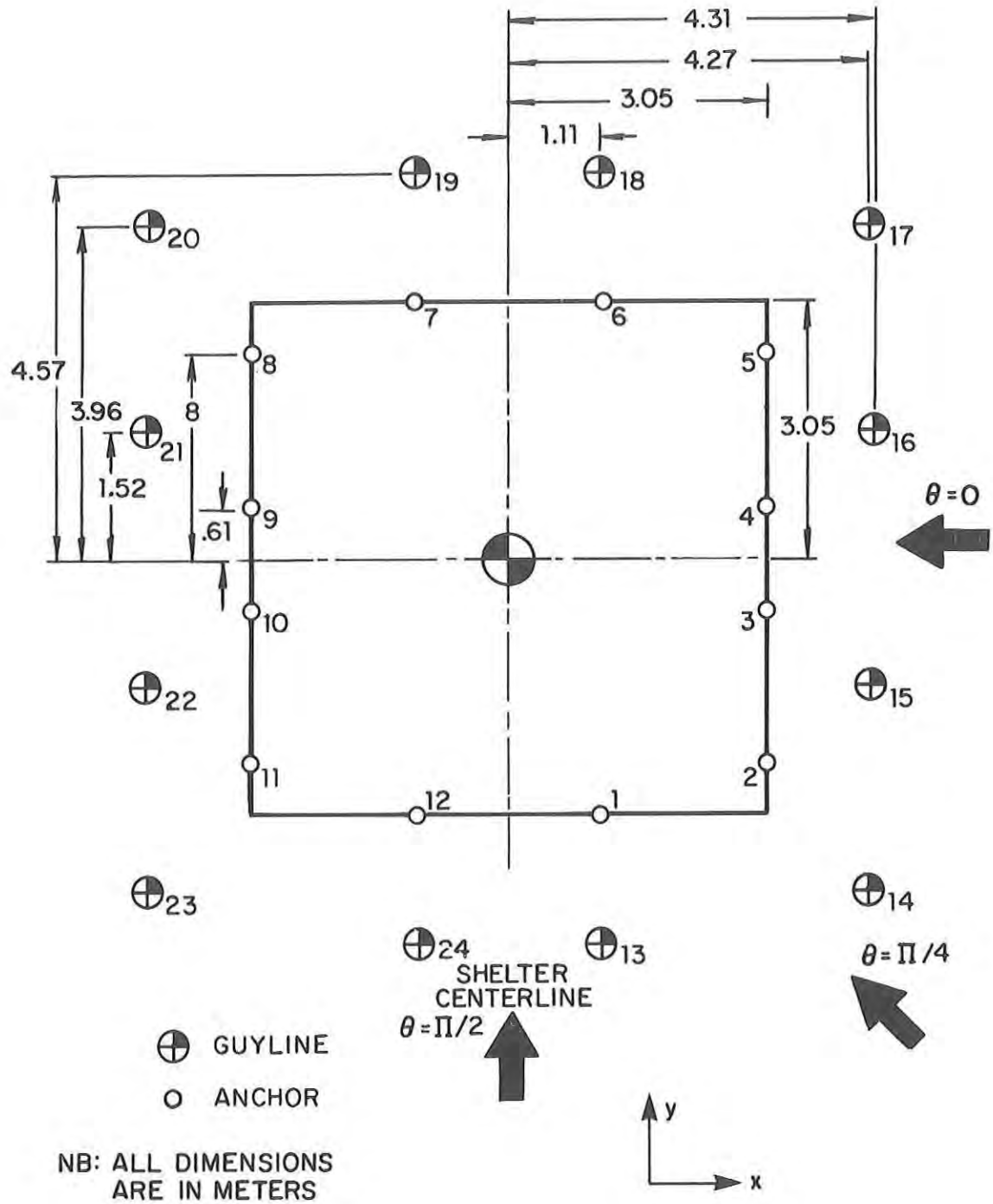

FIG. 2. LOCATION OF FORCE TRANSDUCERS ON DOUBLE-WALL SHELTER.

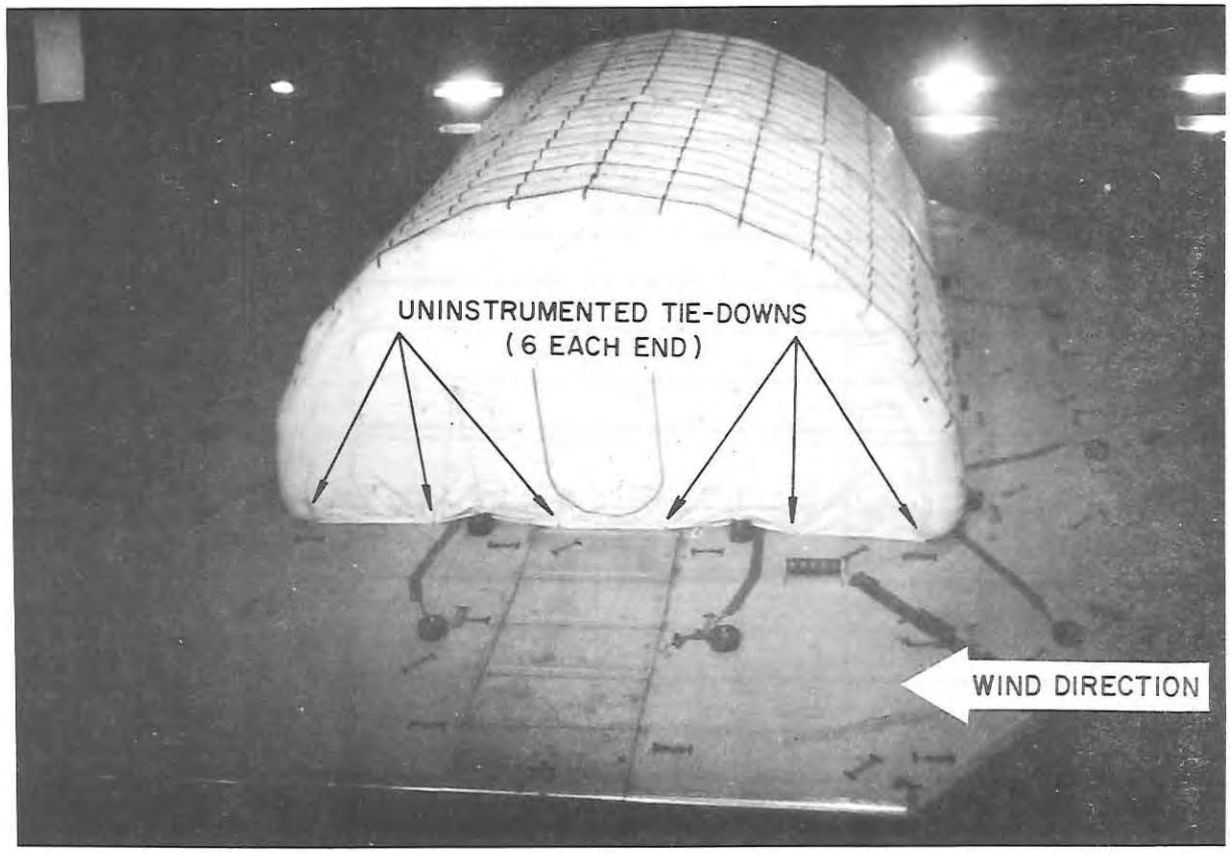

FIG. 3. LOCATION OF UNINSTRUMENTED END-WALL TIE-DOWNS (0° ORIENTATION). [PHOTO COURTESY OF NASA AMES RESEARCH CENTER.]

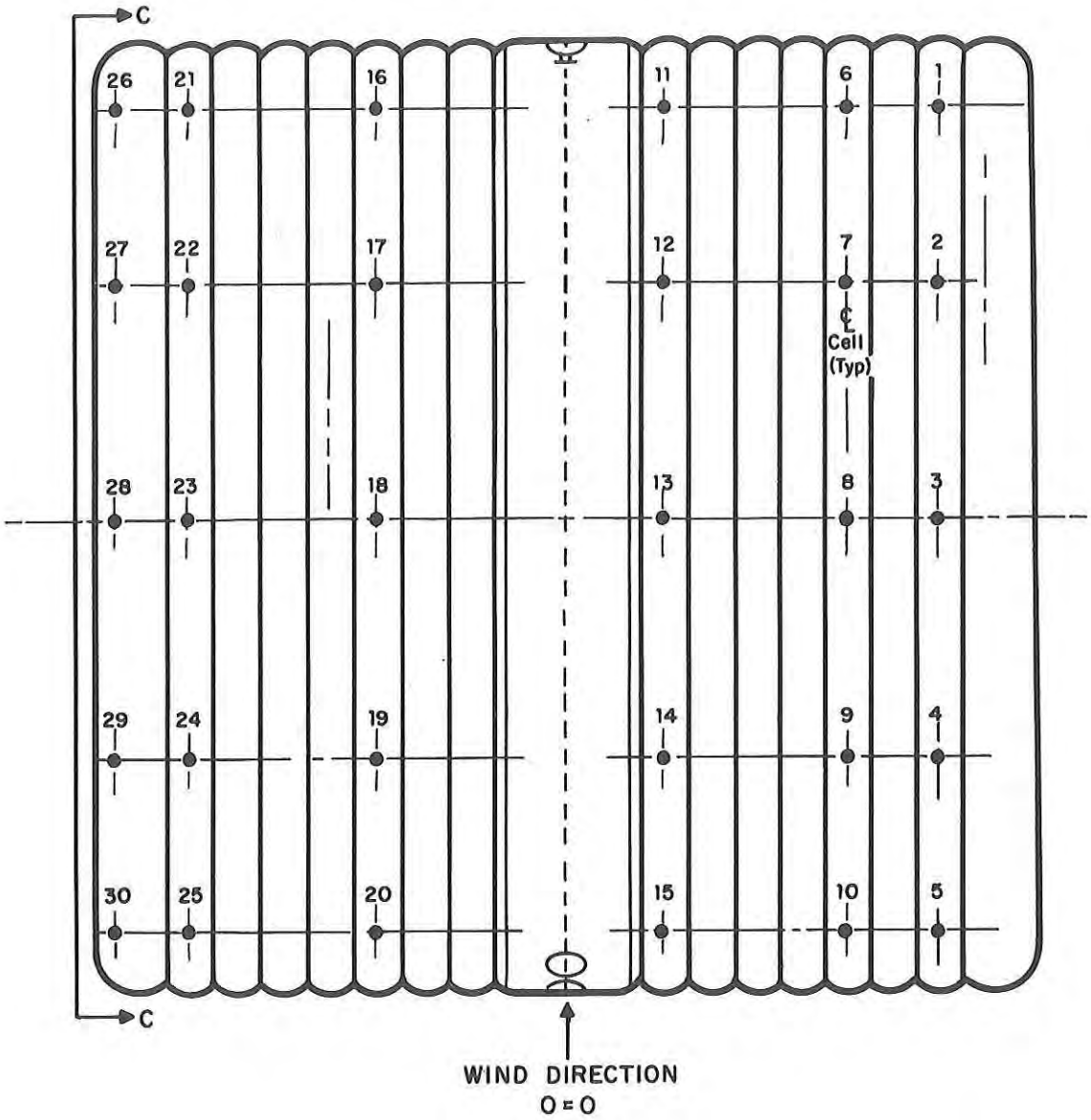

FIG. 4a. LOCATION OF PRESSURE TAPS ON SIDES OF DOUBLE-WALL SHELTER.

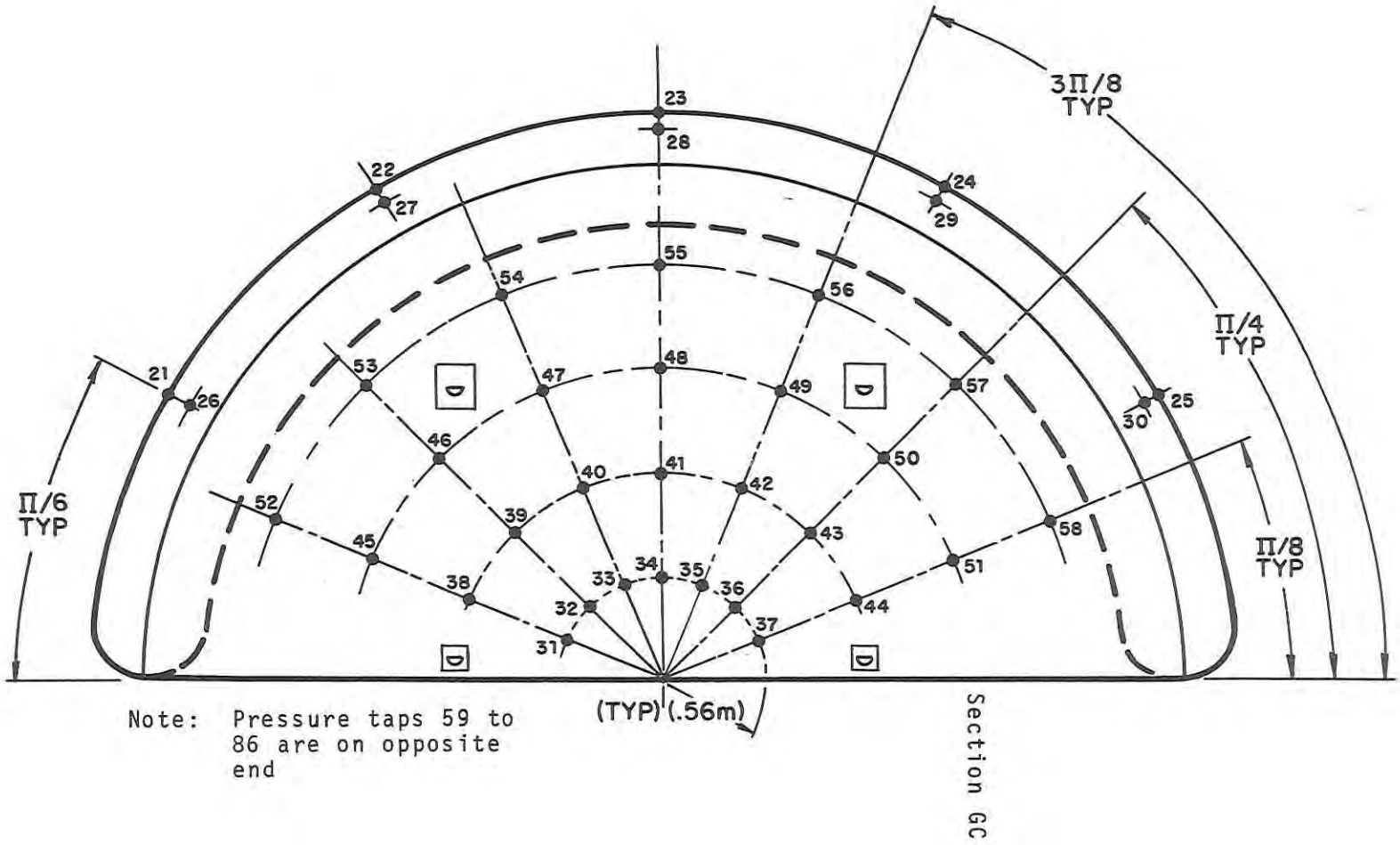

Note: Pressure taps 59 to 86 are on opposite end

FIG. 4b. LOCATION OF PRESSURE TAPS ON END WALLS OF DOUBLE-WALL SHELTER.

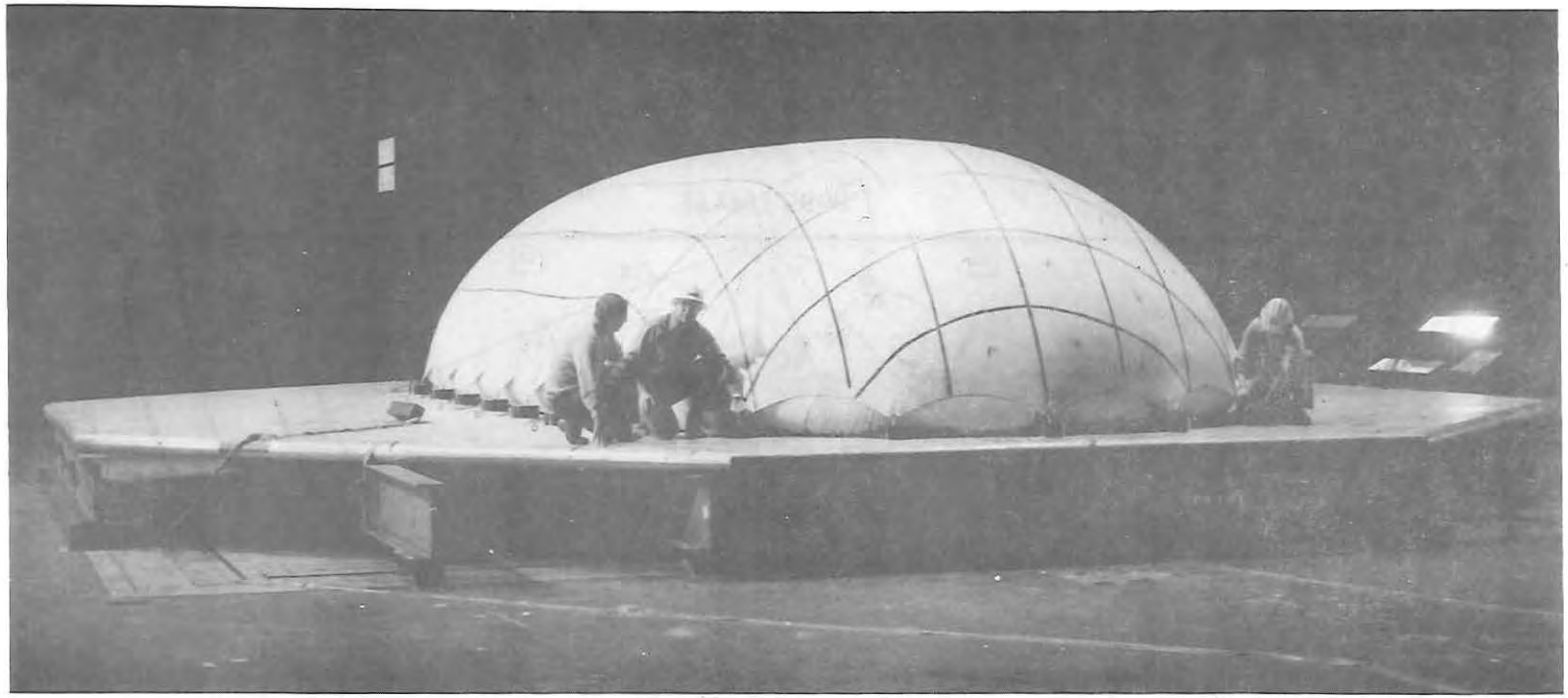

FIG. 5. SINGLE-WALL SHELTER MOUNTED ON GROUND PLANE. [PHOTO COURTESY OF NASA AMES RESEARCH CENTER.]

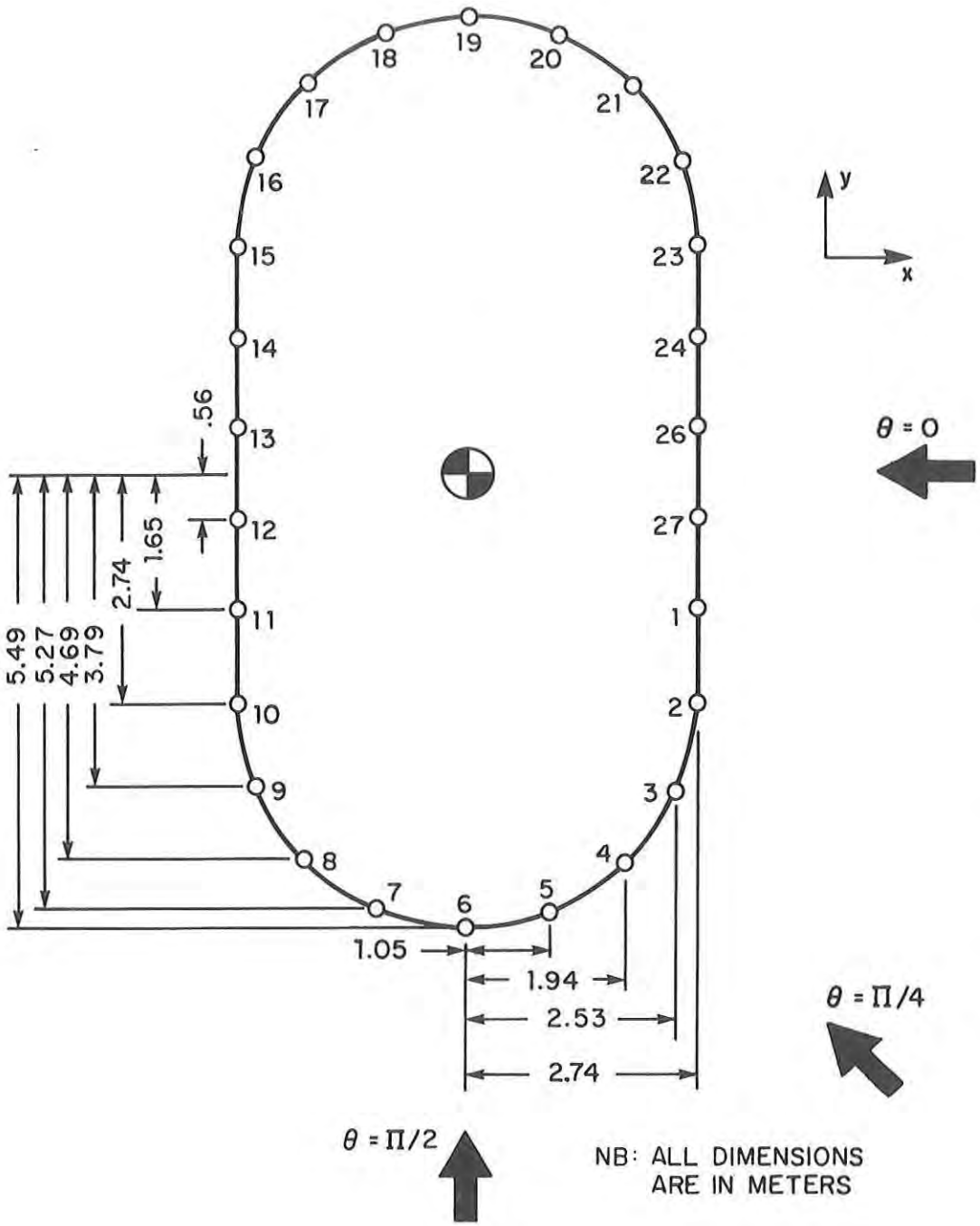

FIG. 6. LOCATION OF FOUR TRANSDUCERS ON SINGLE-WALL SHELTER.

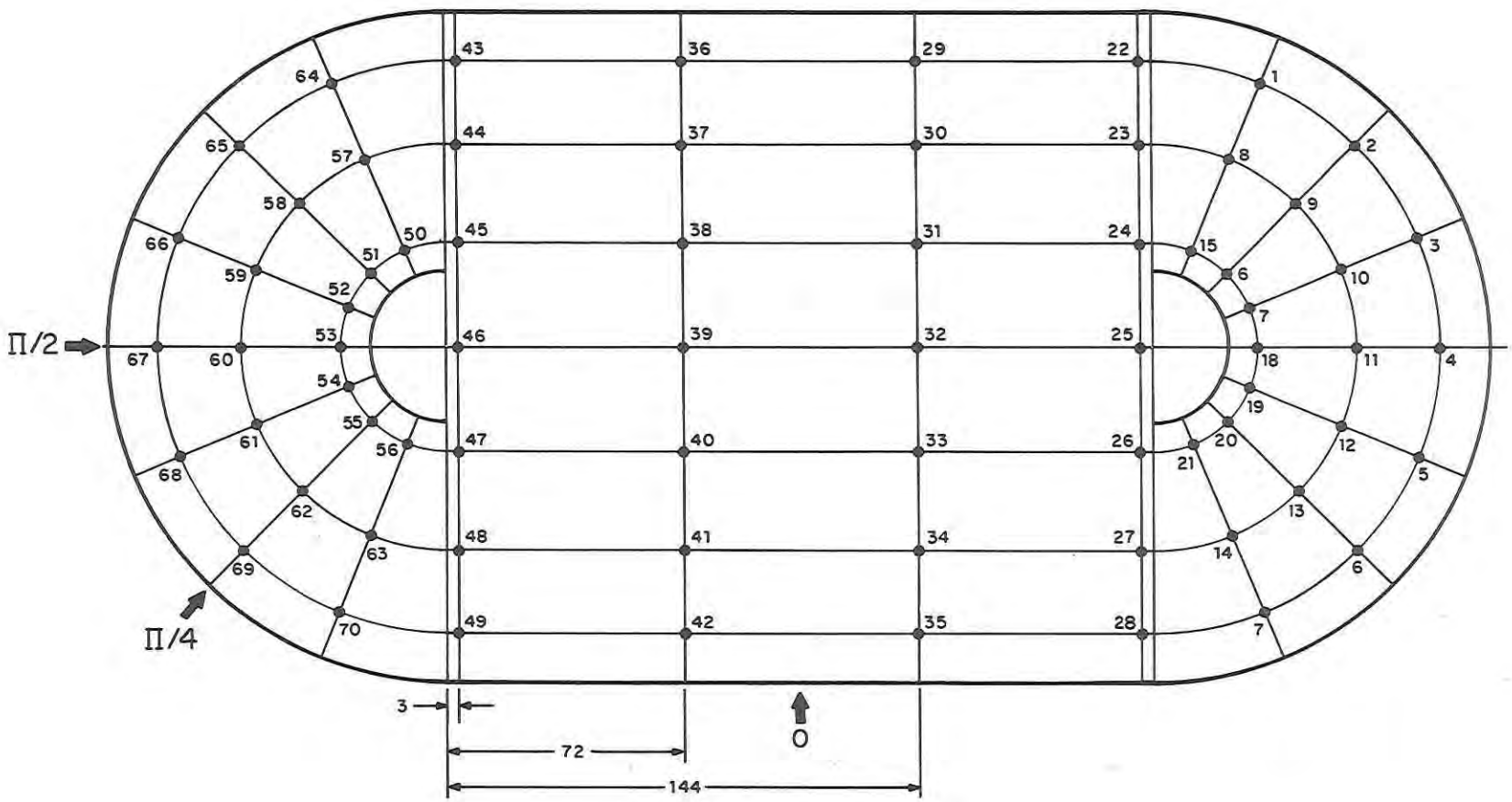

FIG. 7. LOCATION OF PRESSURE TAPS ON SINGLE-WALL SHELTER.

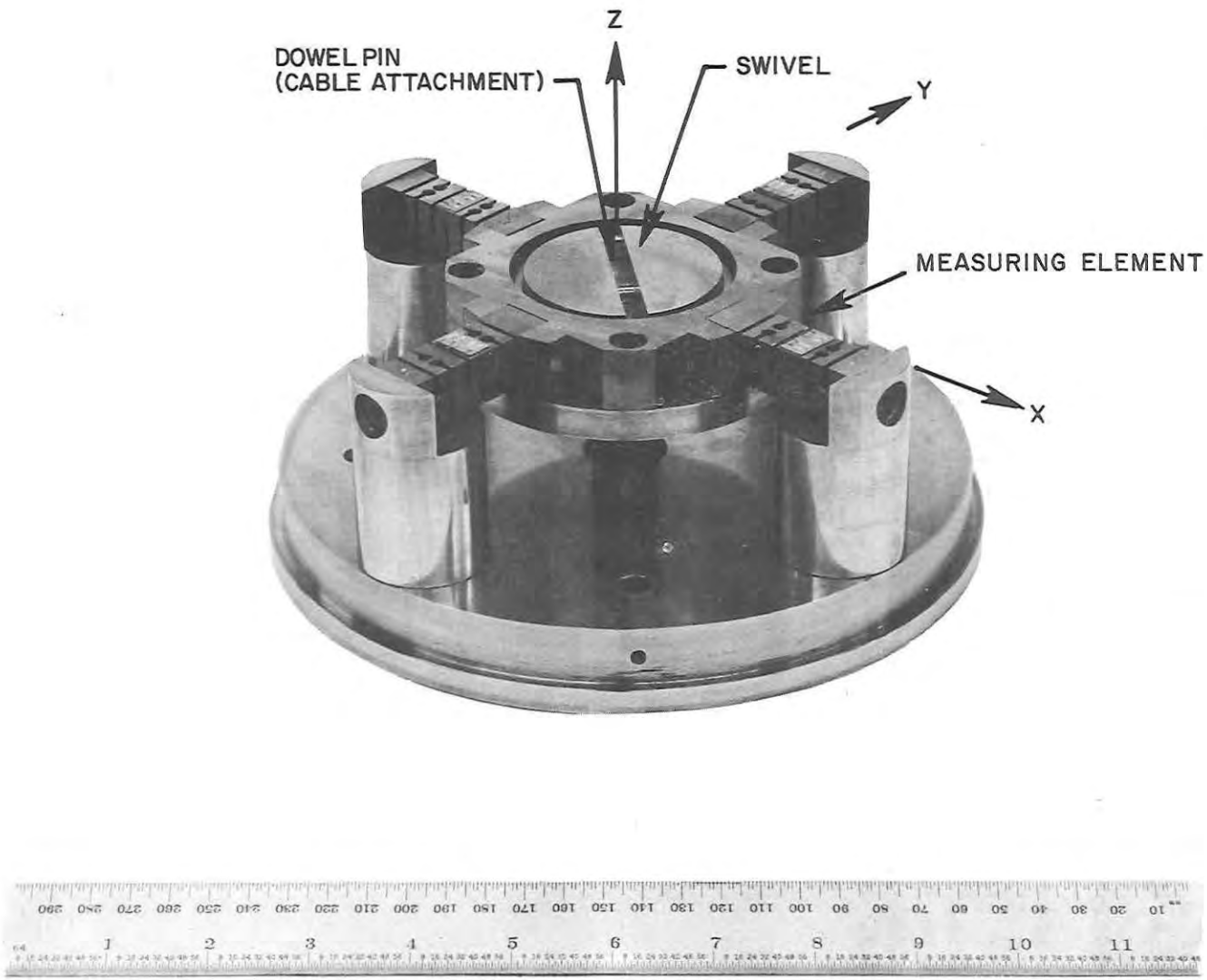

FIG. 8. THREE COMPONENT LOAD TRANSDUCER WITH COVER REMOVED.

2.4.2 Pressure distribution

The surface pressures were transmitted from the shelter surface by flexible tubing to a pair of 48-port scanning valves, fitted with strain-gauge pressure transducers. The long lengths of flexible tubing limited the upper frequency response of the pressure measurement system to less than 1 Hz. Consequently, the pressure data were averaged over a period of 0.5 sec at each port. Calibration was provided by applying a known pressure at one of the ports.

2.4.3 Acceleration

An accelerometer was mounted on each shelter at the 2/3 height in the x-z plane at a position near the geometric center of the shelter. Miniature accelerometers (1.8 gr) were chosen in order not to mass-load the fabric and thus invalidate the acceleration measurement. The upper and lower cutoff frequencies for the accelerometer (±3dB) are 2 and 40,000 Hz, respectively.

3. DATA ACQUISITION AND REDUCTION

3.1 Data Acquisition

The data acquisition system (Fig. 9) consisted of transducers for measuring acceleration, surface pressure, and tie-down loads, together with their associated signal-conditioning electronics, multiplexing, and recording equipment. The recording equipment for acceleration and tie-down loads was a 14-track tape recorder. The noise floor of the system was less than 1% of the value set as full-scale on the recording system. The surface pressure data were recorded on the NASA Ames DATEX II system.

Frequency-domain multiplexing was used in the recording of the tie-down load data. Multiplexed data occupied nine tracks of the tape recorder. A single track contained data from three load cells, which was multiplexed on IRIG proportional bandwidth channels 8 to 16. In addition, a 60-kHz signal was recorded on each track. This signal was used for tape-speed compensation by the demultiplexer. The tracks of the tape recorder were operated in the direct mode. The accelerometer occupied another track, which was operated in the FM mode. Additional channels were used to record an IRIG B time code, a 25-kHz reference signal, and voice. The tape recorder was run at 38.1 cm/sec. The load cell data acquisition system, exclusive of the tape recorder, was mounted in a single standard 48.2 cm rack, located in the control room. The surface pressure ports were coupled to two scanning valves, equipped with strain-gauge pressure transducers. Data from the scanning valves were fed into the NASA Ames DATEX II system, which provided output data both in hard copy and in punched cards.

3.2 Data Reduction

Tie-down loads from the transducers were multiplexed and stored on magnetic tape. These multiplexed analog data were demultiplexed, bandlimited to 50 Hz, and then digitized at 100-Hz sample rate. The resultant digital data were later processed by a digital computer to obtain statistical measures of the loads. Acceleration levels were recorded broadband on the 14-track instrumentation tape recorder. Later, these acceleration waveforms were spectrally analyzed over the frequency band 0 to 500 Hz in 1-Hz analysis bands, using a real-time spectrum analyzer that averaged over 16 samples.

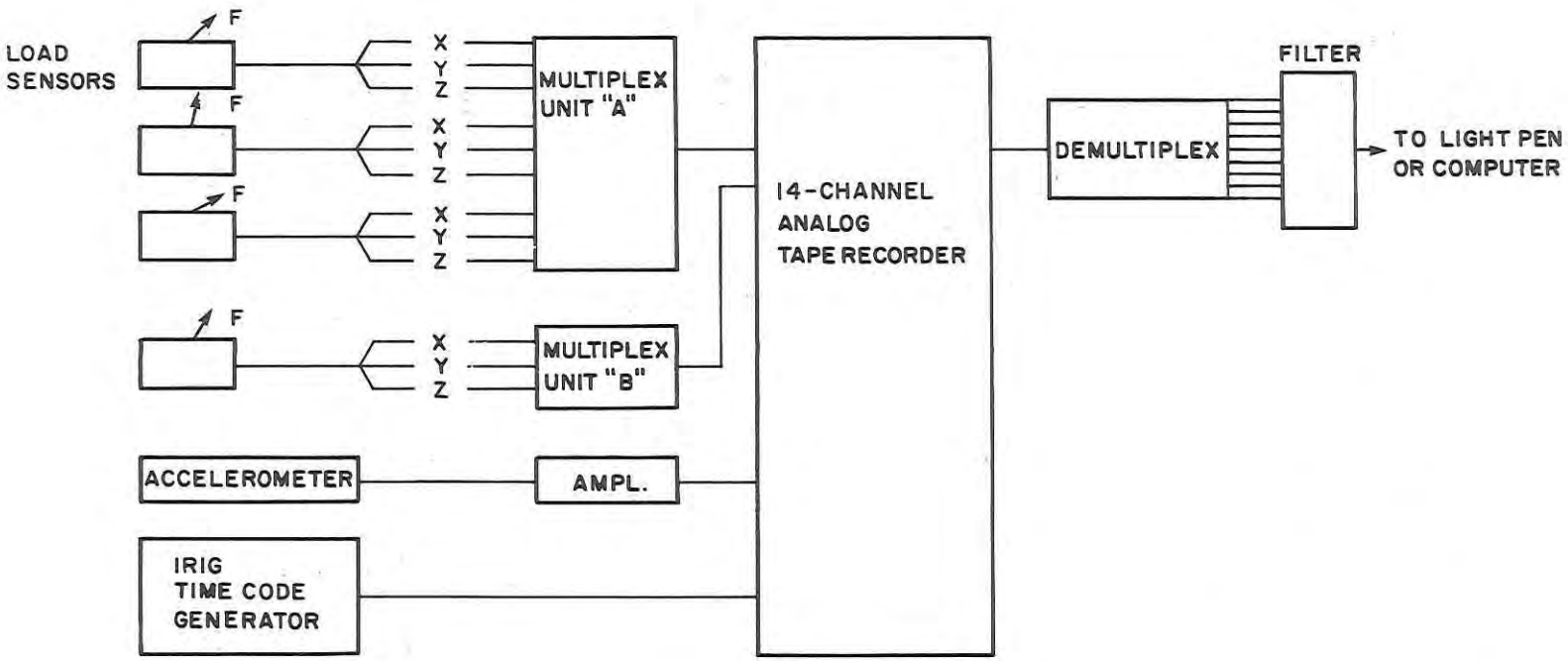

FIG. 9. DATA ACQUISITION SYSTEM.

4. SUMMARY OF TEST CONDITIONS

Tests were conducted at orientations of 0, $\pi/4$, and $\pi/2$ radians to the wind on both the single- and double-wall shelters at velocities up to approximately 49.6 m/sec. The orientations are defined in Figs. 2 and 5 for the double- and single-wall shelters, respectively. At each of these orientations, the wind speed and internal pressure were varied. The following two tables give the test matrix for the double- and single-wall shelters. The test conditions were chosen in a manner similar to that of Ref. 1.

TABLE 1. SUMMARY OF DOUBLE-WALL TEST CONDITIONS.

Run No.	Internal Pressure		Tunnel Pressure		Reynolds No.	Orientation
	in H_2O	N/m^2	psf	N/m^2	$\times 10^{-6}$	rad.
1	20	4980	3.2	153	6.2	0
2			13	622	12.4	
3			20	958	15.6	
4			30	1436	19	
5	15	3735	3.1	148	6.2	
6			23	622	12.4	
7			20	958	15.6	
8			30	1436	19	
9	10	2490	3.1	148	6.2	
10			13	622	12.4	
11			30	1436	19	
12	20	4980	3.2	153	6.2	$\pi/4$
13			13	622	12.4	
14	15	3735	3.2	153	6.2	
15			13	622	12.4	
16			20	958	15.6	
17			30	1436	19	
18	20	4980	30	1436	19	
19	10	2490	3.1	148	6.2	
20			13	622	12.4	
21			30	1436	19	
22	20	4980	3.2	148	6.2	$\pi/2$
23			13	622	12.4	
24			30	1436	19	
25	15	3735	3.1	148	16.2	
26			13	622	12.4	
27			30	1436	19	
28	10	2490	3.1	148	6.2	
29			13	622	12.4	
30			30	1436	19	

TABLE 2. SUMMARY OF SINGLE-WALL TEST CONDITIONS

Run No.	Internal Pressure		Tunnel Pressure		Reynolds No.	Orientation
	in H_2O	N/m^2	psf	N/m^2	$\times 10^{-6}$	rad.
1	$2\frac{1}{8}$	529	8.3	397	2.1	$\pi/2$
2			10.4	498	10.6	
3			13	622	11.6	
4	4	996	16.6	795	13.1	
5			20.8	996	14.6	
6			26	1245	16.4	
7			20.8	996	14.6	
8			26	1245	16.4	
9	5	1245	20.8	996	14.6	
10			25.8	1235	16.4	
11			32.5	1556	18.6	
12	2	498	8.3	397	9.1	$\pi/4$
13			10.4	498	10.6	
14			13	622	11.6	
15	4	996	16.6	795	13.1	
16			20.8	996	14.6	
17			26	1245	16.4	
18	5	1245	26	1245	16.4	
19			20.8	996	14.6	
20	2	498	8.3	397	9.1	0
21			10.4	498	10.6	
22			13	622	11.6	
23	4	996	16.6	795	13.1	
24			20.8	996	14.6	
25			26	1245	16.4	
26	5	1245	26	1245	16.4	
27			20.8	996	14.6	

5. RESULTS AND DISCUSSION

Section 5 presents the behavior of single- and double-wall shelters under wind loadings. Overall force coefficients, individual tie-down loads, pressure distributions plus spectra of the tie-down loads, and shelter fabric accelerations are discussed. Comparisons are made with previous work, and comments are included that will assist understanding of shelter behavior.

Data are presented in nondimensional form, using the following parameters:

Force coefficient $C = \frac{F}{qA}$

Lift coefficient $C_L = \frac{F_L}{qA}$

Drag coefficient $C_D = \frac{F_D}{qA}$

Reynolds number $N_R = \frac{VD}{\nu}$,

where F is a force, q is the wind tunnel dynamic pressure [$q = 1/2\ \rho V^2$], A is the planform area of the shelter, V is velocity, D is shelter diameter, ν is the kinematic viscosity of air, and ρ is the density of air.

5.1 Double-Wall Shelter

5.1.1 Loads

The lift and drag coefficients as a function of Reynolds number are presented in Fig. 10 for the double-wall shelter at an orientation of 0. The figure is a composite of tests run at various values of internal pressure, with the range of values obtained indicated by bars. The figure illustrates that the drag coefficient is independent of wind speed for the range of wind speeds tested and has a value of $C_D \approx .18$. The lack of dependence on Reynolds number is to be expected, since at even the lowest velocity the Reynolds number was greater than 10^6. One possible explanation for the spread in data at the lowest Reynolds number starts with noting

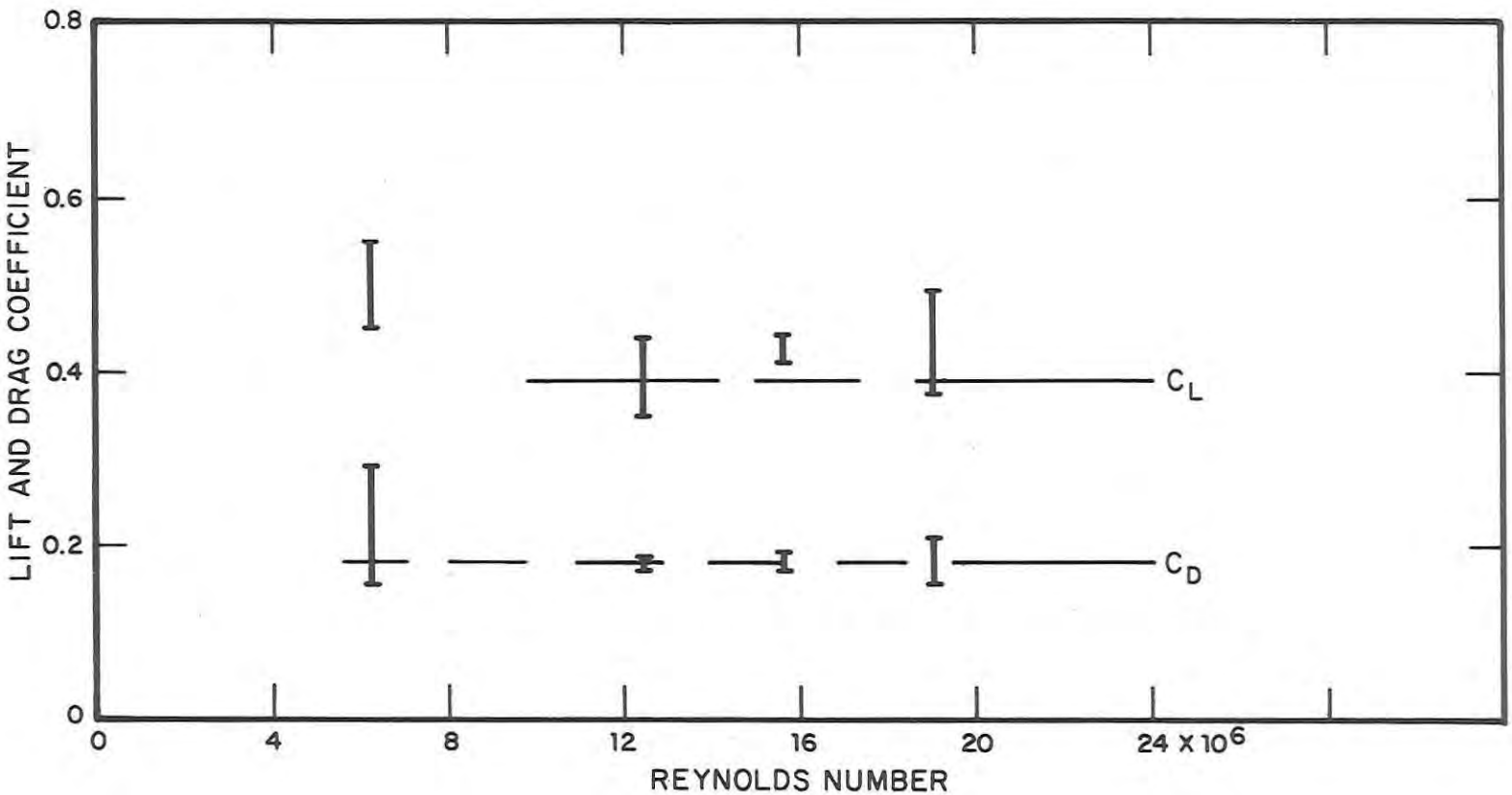

FIG. 10. LIFT AND DRAG COEFFICIENT AS A FUNCTION OF REYNOLDS NUMBER.

that the initial test gave the low value, and the two subsequent tests gave the higher value. As indicated in Table 1, a number of higher Reynolds number tests were conducted between the times when the low Reynolds number tests were run. It is postulated, then, that loading on the shelter at the high Reynolds number caused it to slide slightly downstream and that the shelter could not return to its original position because of friction between the tent and the ground plane. This frictional force accounts for the differences between the coefficients at the low Reynolds number. Although the frictional component is still present at the higher Reynolds number, its effect on drag coefficient is attenuated by the nondimensionalization procedure. The lift coefficient is also virtually independent of Reynolds number at the higher Reynolds number tests and has a value of $C_L \approx 0.38$. There is, however, more scatter in the measured values at a given Reynolds number than is exhibited in the drag. Of particular interest is the variation in the lift coefficient at the highest Reynolds number. [Two of the tests gave similar coefficients (C_L = 0.39 and 0.37); the highest Reynolds number test gave C_L - 0.49.] This variation is explained by the fact that prior to, or during, the test that had the highest lift coefficient, the uninstrumented end-wall tie-downs pulled out of the fabric, and the load that they would customarily carry was transferred to the surrounding load cells. The anchor loads for both cases are shown in Fig. 11. Figure 11 shows that when the uninstrumented tie-downs tore loose, their load was taken up, primarily, by the end-walls load cells and, to a minor degree, by the corner load cells in the windward direction. A comparison of the lift coefficients for both cases indicates that for the 0 orientation, the uninstrumented tie-downs make a contribution of 0.1 to the lift coefficient (i.e., 20%). This is an important contribution, and we recommend that these tie-downs be instrumented in future tests.

Figure 12 presents a comparison of force coefficients between the present test program, maximum values from a previous program [*1*] on scale models of double-wall shelters, and a rigid body program [*5*] on similar structures. Note that both of the previous programs were conducted at lower Reynolds numbers than the present program, which may account for some differences in the data. An attempt was made in the rigid body program to raise the Reynolds number artificially by using a boundary layer trip wire, but it is not possible for us to determine how effective this was. In Fig. 12, consider first the graph of C_y (force along the

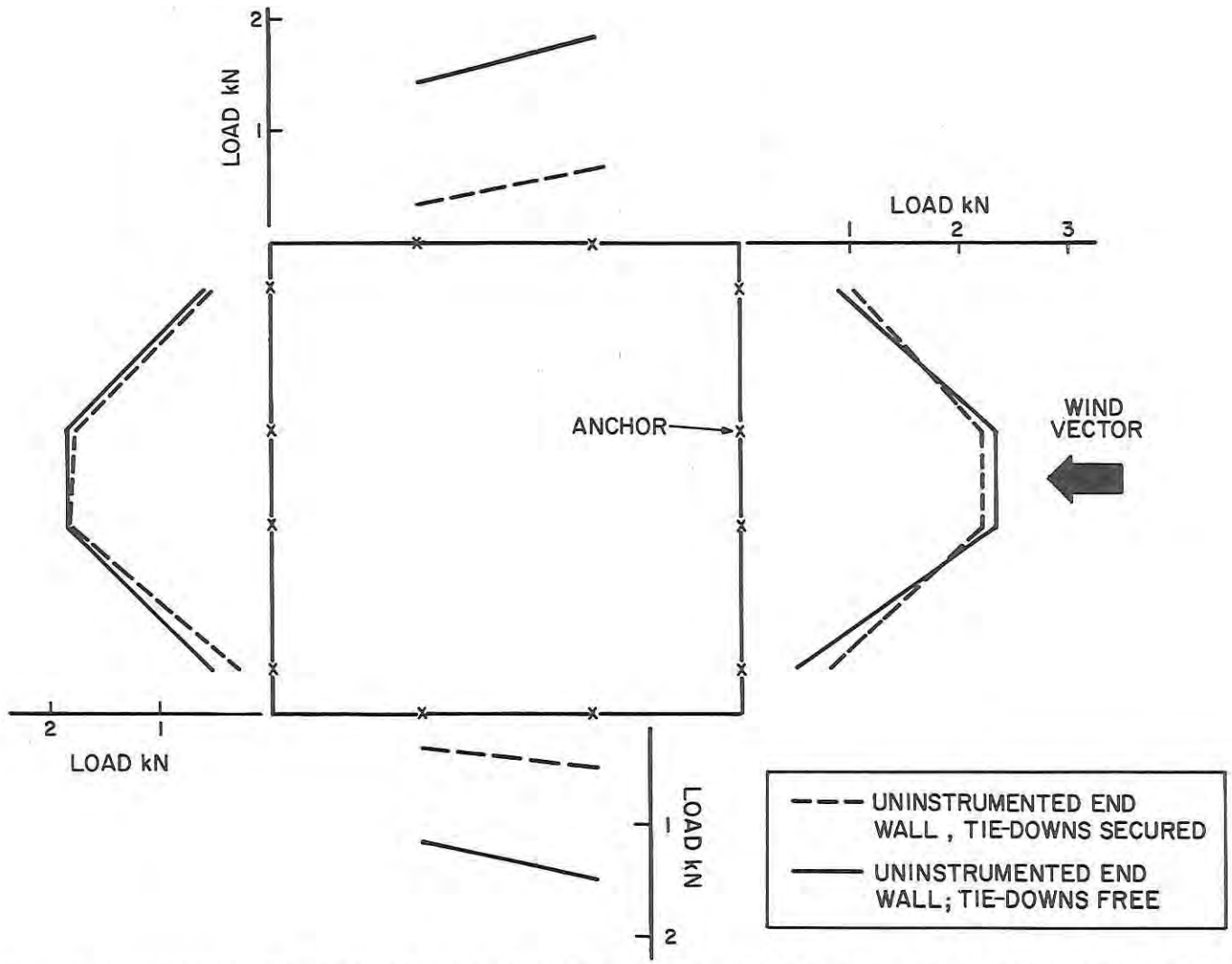

FIG. 11. COMPARISON OF ANCHOR LOADS WITH AND WITHOUT END-WALL GROMMETS ATTACHED TO GROUND PLANE.

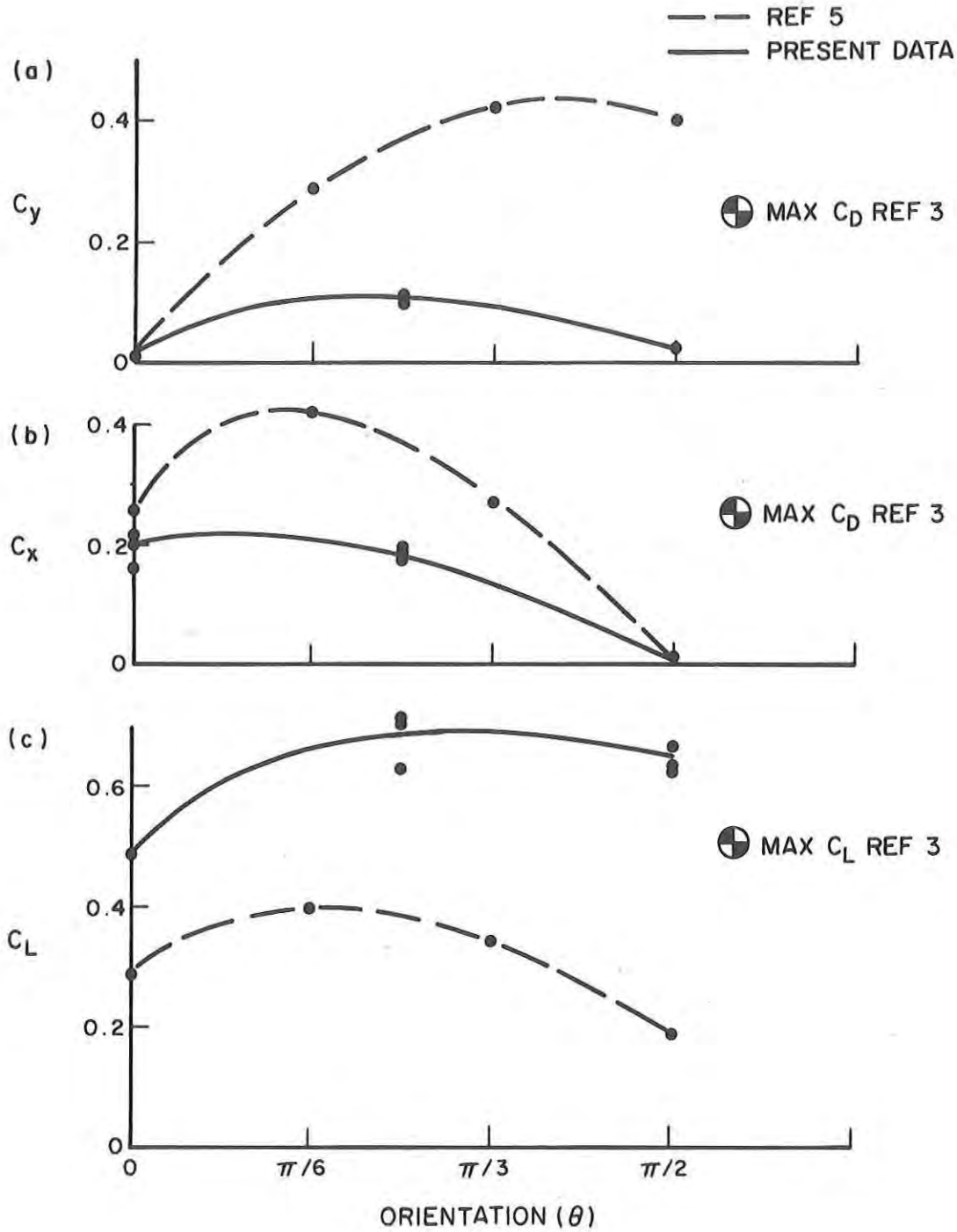

FIG. 12. SUMMARY OF FORCE COEFFICIENTS AT $N_R = 19 \times 10^6$ AS A FUNCTION OF ORIENTATION.

shelter axis) as a function of orientation. As expected, both the present and the previous data pass through zero at the 0 orientation. However, for other orientations, the results are markedly different. Note, also, that the results of a previous test on flexible structures gave a maximum drag coefficient that is somewhat lower than the rigid body results. Some of the difference between present results and the previous flexible body results is clearly attributable to the loads carried by the uninstrumented tie-downs on the end wall. Considering C_x, the values for the rigid structure and the present double-wall structure correspond closely at both the 0 and $\pi/2$ orientation and deviate substantially at $\pi/4$. Again, some of this variation would be attributable to the end-wall tie-downs and to the difference between rigid and flexible structures. The lift coefficients are compared in part C of the figure. Note that the effects of the uninstrumented tie-downs are not included, and consequently the measured coefficients may be low.* Again, we note a large discrepancy between the rigid body results and the flexible body results. In addition, we note that the present results are higher than the maximum results measured during a previous scale-model program. Two possible explanations are offered for the differences at this stage: (1) air leaking through the zipper or another opening in the shelter, causing an effective pressurization, and (2) stagnated air leaking under the tent floor, causing a load on the tie-downs.

We cannot ascertain which of the two possibilities is predominant; consequently, we recommend that a further test program be conducted to determine the source of the discrepancy.

We do, however, feel that the latter explanation – stagnated air under the tent floor – is more plausible, since the maximum deviation between the previously measured lift coefficient and the present result occurs at $\pi/4$ and $\pi/2$, where the end walls (which are poorly coupled to the ground) are directly exposed to the wind.

Figure 13 shows the anchor and guyline coefficients as a function of Reynolds number. The figure is a composite of all tests excluding the lowest velocity tests, which were

---

*Integration of the pressure profile over the shelter surface gives a larger lift coefficient than that measured, which confirms the contribution of the uninstrumented tie-downs.

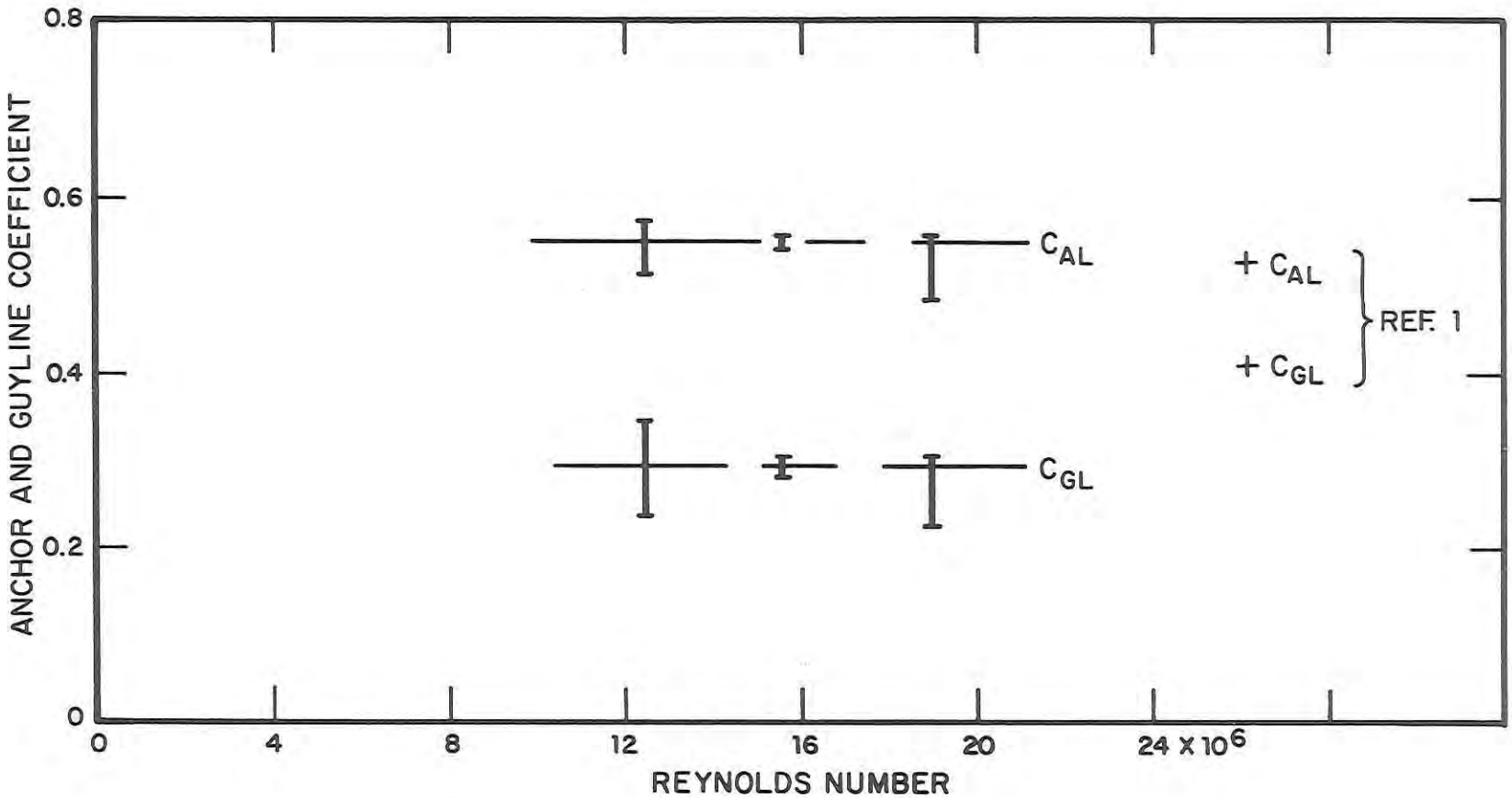

FIG. 13. ANCHOR AND GUYLINE COEFFICIENTS AS A FUNCTION OF REYNOLDS NUMBER.

omitted because of the large amount of scatter caused by low loads.

The anchor coefficient compares well with the results of the previous program [1]. However, the guyline coefficents are lower in the present test. This discrepancy is no doubt attributable to the fact that Ref. 1 used a maximum individual load in establishing the anchor and guyline coefficients. The present results are for total load, and a simple check shows that $C_{AL} + \sin\theta C_{gL} \approx C_L$, where θ is the angle between the vertical and the guylines ($\pi/4$). The coefficients based on total load should be viewed as a mean value, and it would be instructive, at this point, to consider the individual loads to ascertain the variance about the mean.

Figures 14a, b, and c present the coefficients associated with the vertical components of anchor and guyline load at $N_R = 19 \times 10^6$ for the orientations $\theta = 0$, $\pi/4$, and $\pi/2$, respectively. Each plot is composed of three curves representing internal pressures of 2490, 3735, and 4980 N/m^2. The wind direction is also given in each figure.

Figure 14a shows the distribution of load at an orientation of 0. The curves for internal pressures of 2490 N/m^2 and 3735 N/m^2 are approximately the same for both anchors and guylines, indicating a lack of dependence on internal pressure. The anchor loads for $P_i = 4980$ N/m^2 are significantly different; however, this difference is attributed to the breaking of the uninstrumented tie-downs and not to internal pressure. It is interesting to note that the breaking of the uninstrumented tie-downs had virtually no effect on the guyline loads. Consequently, we can conclude that there was no gross deformation or displacement of the shelter as a result of the tie-down breakage. Figures 14b and 14c again illustrate the independence of load on internal pressure. In addition, 14b shows that the maximum load occurs at the $\pi/4$ orientation.

Figure 15 summarizes the results of the previous figures and also presents the maximum loads which occur on both guylines and anchors. The test conditions at the three orientations have been extrapolated to cover other orientations through the use of symmetry arguments (e.g., the peak load on tie-downs 1 and 12 for the $\pi/2$ orientation would occur on tie-downs 6 and 7 for a $-\pi/2$ orientation). One ordinate of each graph is the anchor load normalized by dynamic pressure times surface area divided by the appropriate coefficient

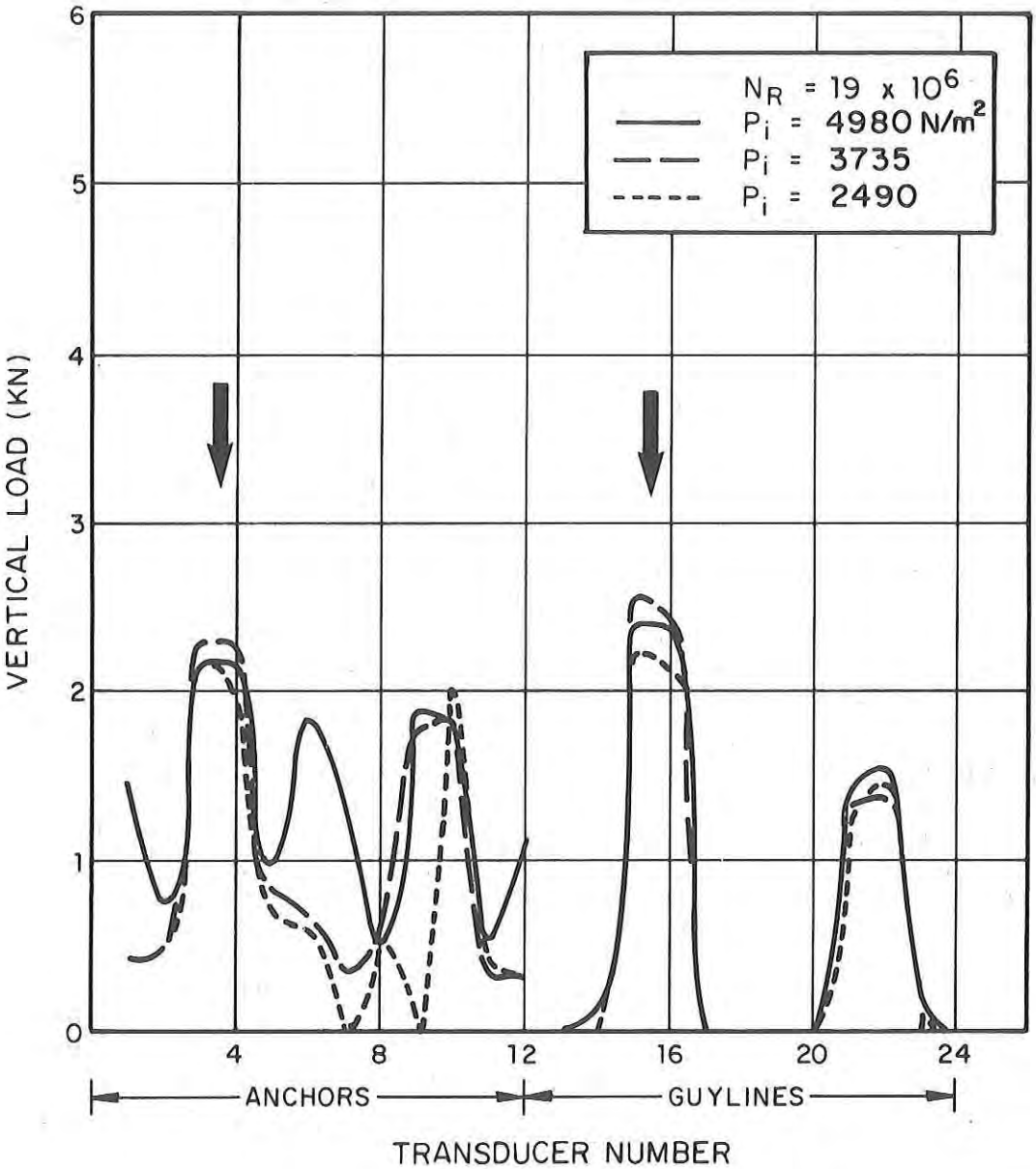

FIG. 14a. DISTRIBUTION OF GUYLINE AND ANCHOR LOAD AT $\theta = 0$.

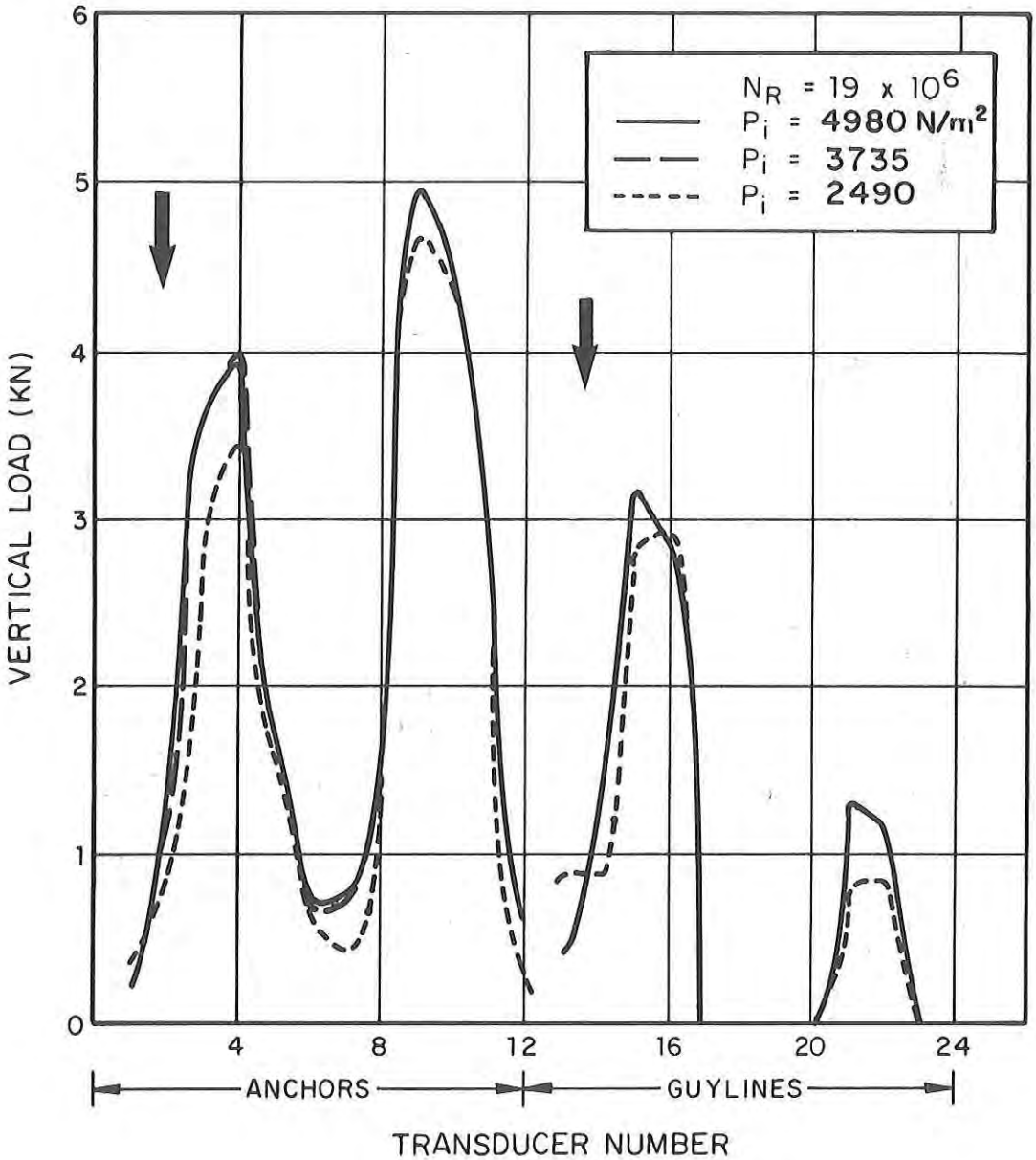

FIG. 14b. DISTRIBUTION OF ANCHOR AND GUYLINE LOAD AT $\theta = \pi/4$.

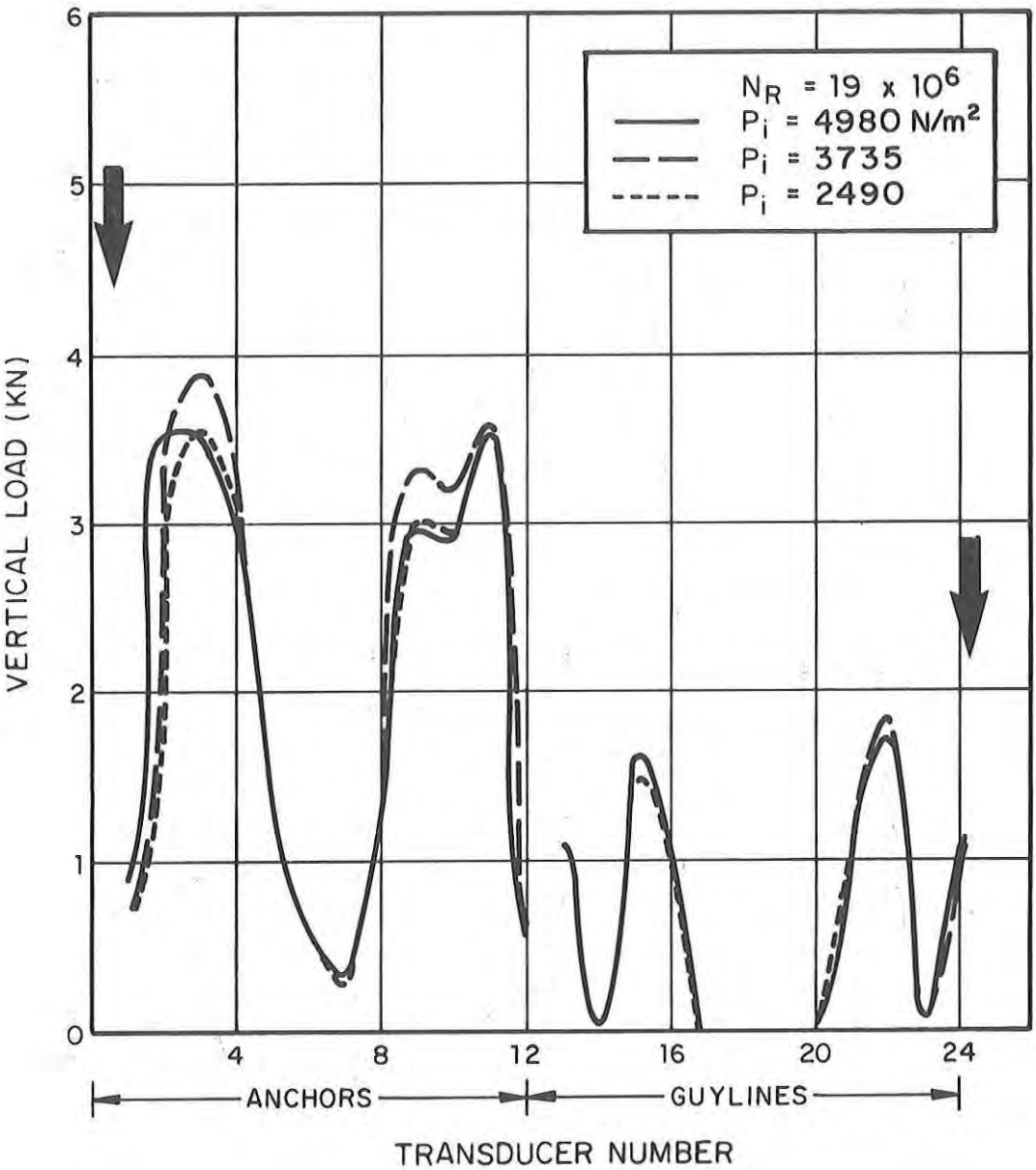

FIG. 14c. DISTRIBUTION OF ANCHOR AND GUYLINE LOAD AT $\theta = \pi/2$.

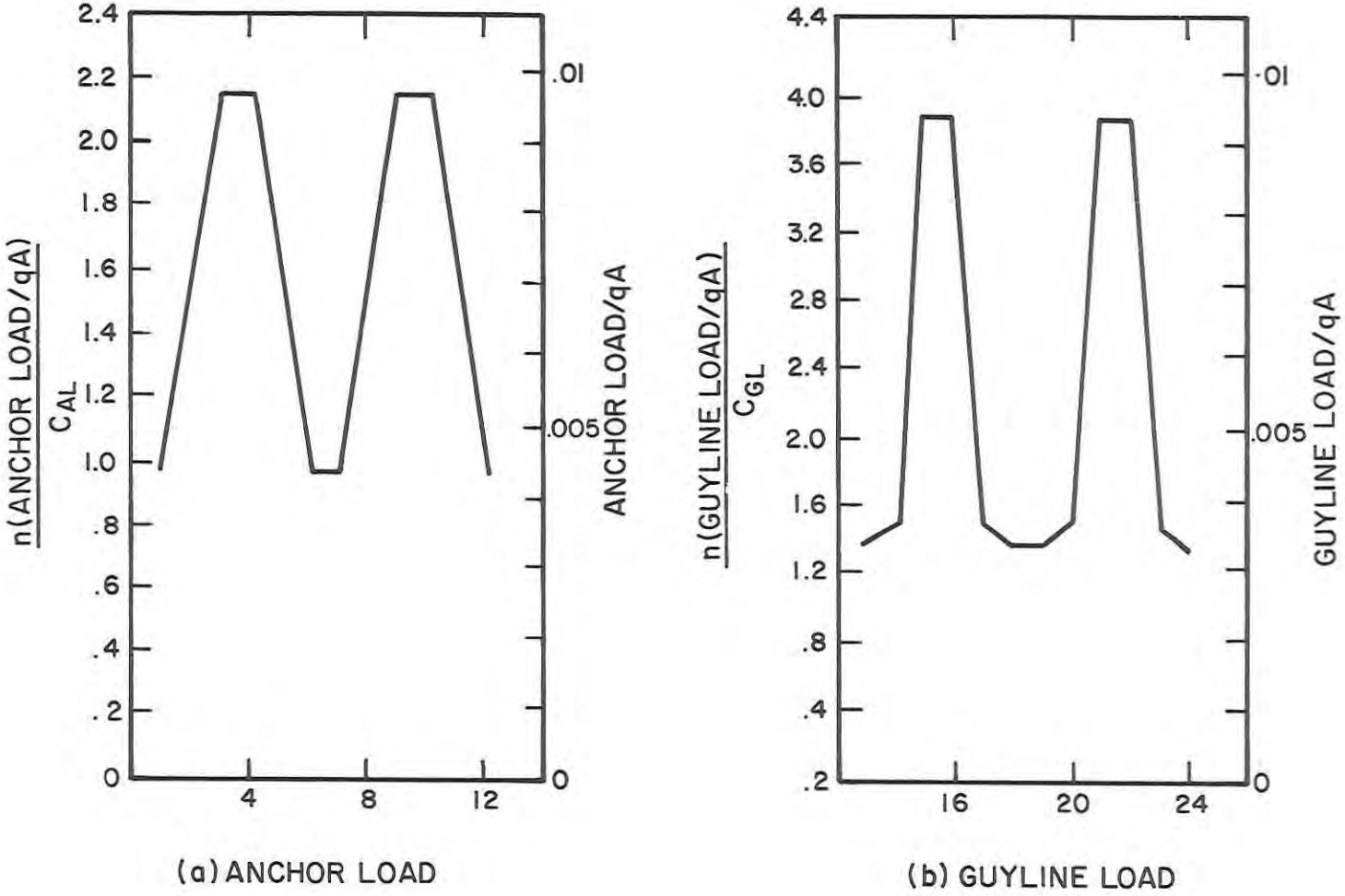

FIG. 15. SUMMARY OF MAXIMUM ANCHOR AND GUYLINE LOAD.

divided by the number of that type of tie-down. This normalization is equivalent to that presented in Ref. 3. Following the procedure given in Ref. 3, and using the anchor coefficient of Fig. 13, the peak anchor load estimate would be in error by a factor of more than 2. Similarly, an estimate for guyline loads would be in error by a factor of 4. The alternate, and perhaps more useful, ordinate is the tie-down load normalized by dynamic pressure times area. It should be emphasized that these curves are a summary of maxima, and, consequently, the total load obtained by summing the individual loads on Fig. 15 would be much higher than that obtained from any given test.

5.1.2 Pressure distributions

Figure 16 presents the circumferential distribution of nondimensional pressure over the shelter surface at the 0 orientation. The data from all tests are specified by bars. The measured data are typical of that measured by taps away from the end wall (i.e., 6 to 25 in Fig. 3). The data are typical of experimental data from rough cylinders.

Figure 17 presents the distribution of nondimensional pressure on the end wall at an orientation of $\pi/2$. Two characteristics are worthy of note. First, the distribution is not symmetrical with respect to the centerline and, second, the average pressure coefficient over the surface is significantly less than 1. The lack of symmetry indicates that the tie-down load distribution should be unsymmetrical. Reference to Fig. 14c does not support this conclusion; consequently, we must assume that the uninstrumented tie-downs are unequally loaded.

The fact that the average pressure coefficient is less than 1 indicates that the drag force should be less than that predicted for the rigid model at $\pi/2$.* This conclusion is borne out by the data.

5.1.3 Spectra of tie-down loads and shelter accelerations

The spectra of typical tie-down loads and of the accelerometer were calculated in 1-Hz bandwidths for a number of

---

*For the rigid model at $\pi/2$, if we assume that the pressure on the end wall is stagnated ($C_p = 1$), the drag coefficient is merely the ratio of the end-wall area to the platform area ($\pi/8$), as shown in Fig. 10.

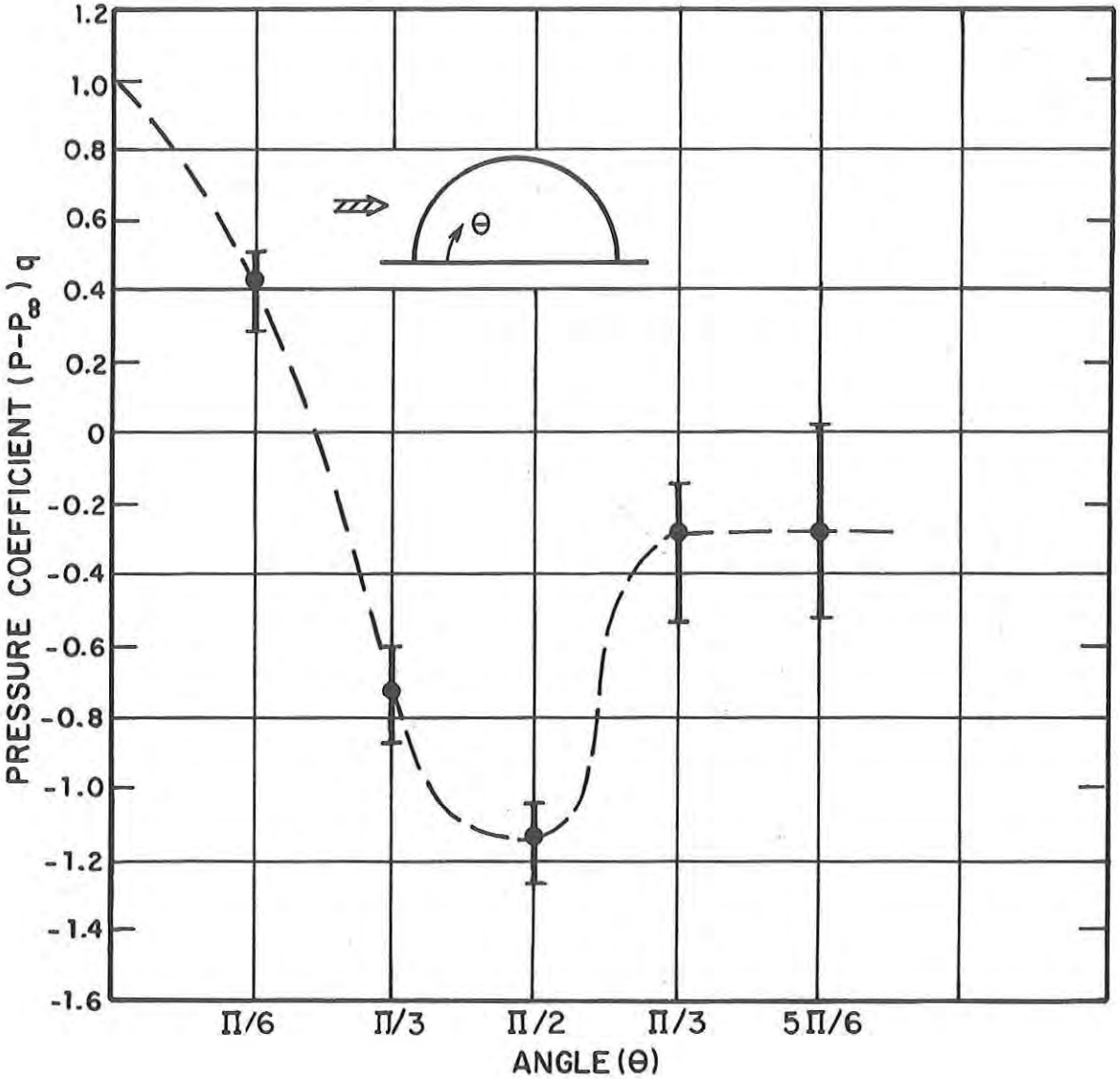

FIG. 16. PRESSURE DISTRIBUTION ON DOUBLE-WALL SHELTER AS A FUNCTION OF ANGLE AT 0 ORIENTATION.

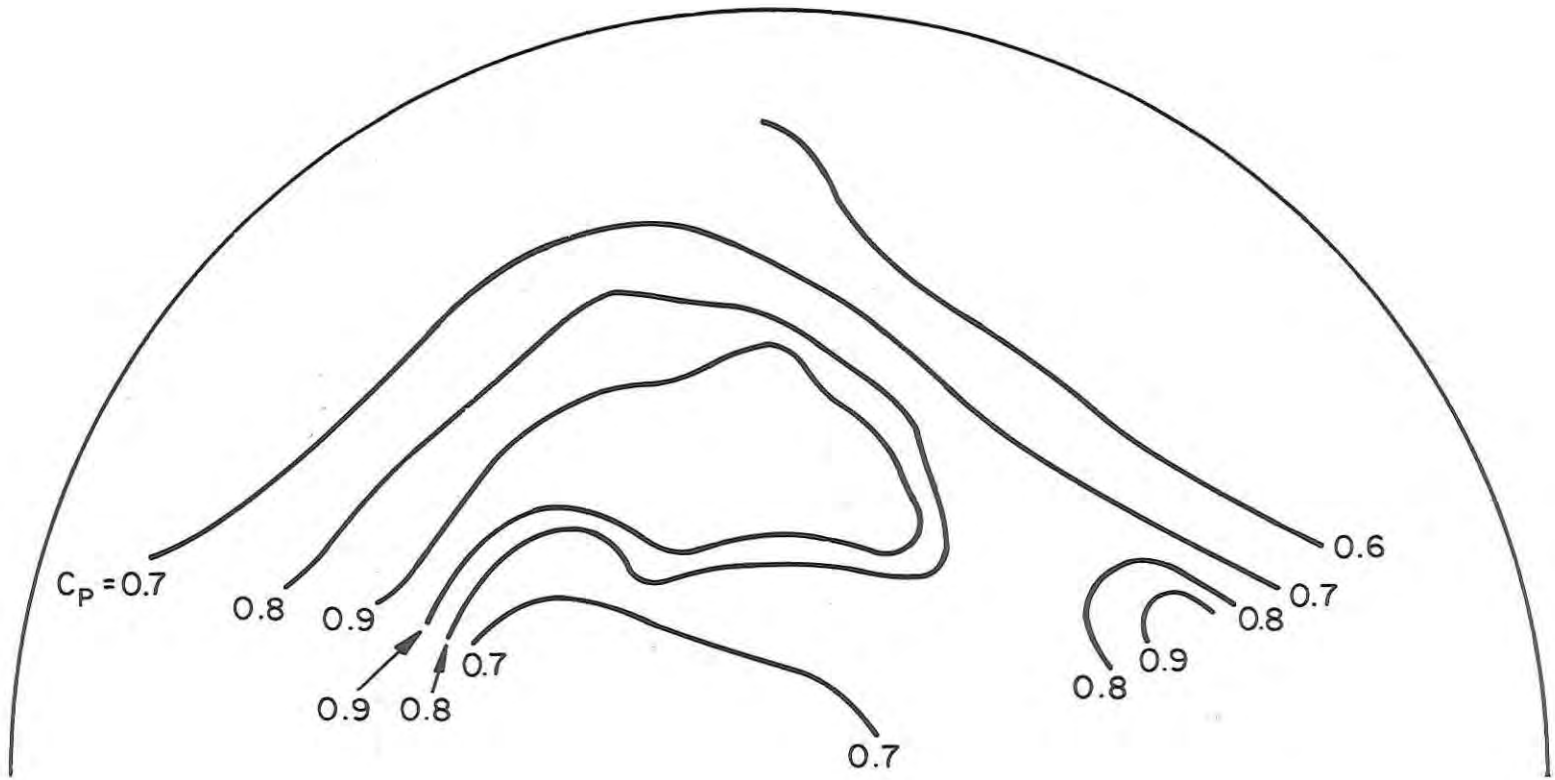

FIG. 17. NONDIMENSIONAL PRESSURE DISTRIBUTION ON SHELTER END WALL AT AN ORIENTATION OF $\pi/2$.

the tests. Figure 18 presents a comparison of the spectra. The ordinate has been chosen to be an arbitrary amplitude squared per Hz so that both curves may be presented together. Note that there is no contribution for frequencies in excess of 18 Hz for the anchor load, and in fact the majority of energy lies below 8 Hz. The fabric accelerations, on the other hand, exhibit a peak at approximately 15 Hz and another relatively broadband peak at 30 Hz. The 30-Hz signal in the fabric is exhibited in all the double-wall tests and is, therefore, thought to be a structural resonance of the shelter. However, it does not appear in the anchor load spectrum and consequently is not of importance in design.

5.2 Single-Wall Shelter

The single-wall shelter tie-down forces are a combination of the load from inflation and the aerodynamic load. The inflation load also has two components: that due to the difference between internal and external pressure prior to startup of the tunnel, and that due to the decrease in external pressure following tunnel startup. Remembering that the static pressure in the tunnel is approximately the atmospheric pressure minus the tunnel dynamic pressure q, the effective inflation pressure becomes $P_{IE} = P_I + q$, where $q = 1/2\ \rho V_\infty^2$ and P_I is the inflation pressure relative to atmospheric, i.e., measured in the control room relative to the control room. The term due to the static pressure drop in the tunnel test section of the present test program is of the same magnitude as the P_I term and, consequently, will have to be considered in reducing the loads to inflation loads and aerodynamic loads. These loads have been separated and are treated individually in the following discussion.

5.2.1 Inflation loads

At zero flow conditions, anchor load measurements were made to permit the extraction of inflation loads from total anchor loads generated during the wind tests. The total vertical anchor load as a function of inflation pressure is shown in Fig. 19. These loads are less than the inflation loads expected on the basis of the shelter planform area of 53.7 m^2. This discrepancy is explained by the fact that the load cells react only to that load which is the product of the internal pressure and the area of the shelter in contact with the floor. The contact area is less than the planform area (Fig. 5) because of curvature of the shelter floor at its edges, and thus the inflation loads are lower than expected. Based on the measured values in Fig. 19, we

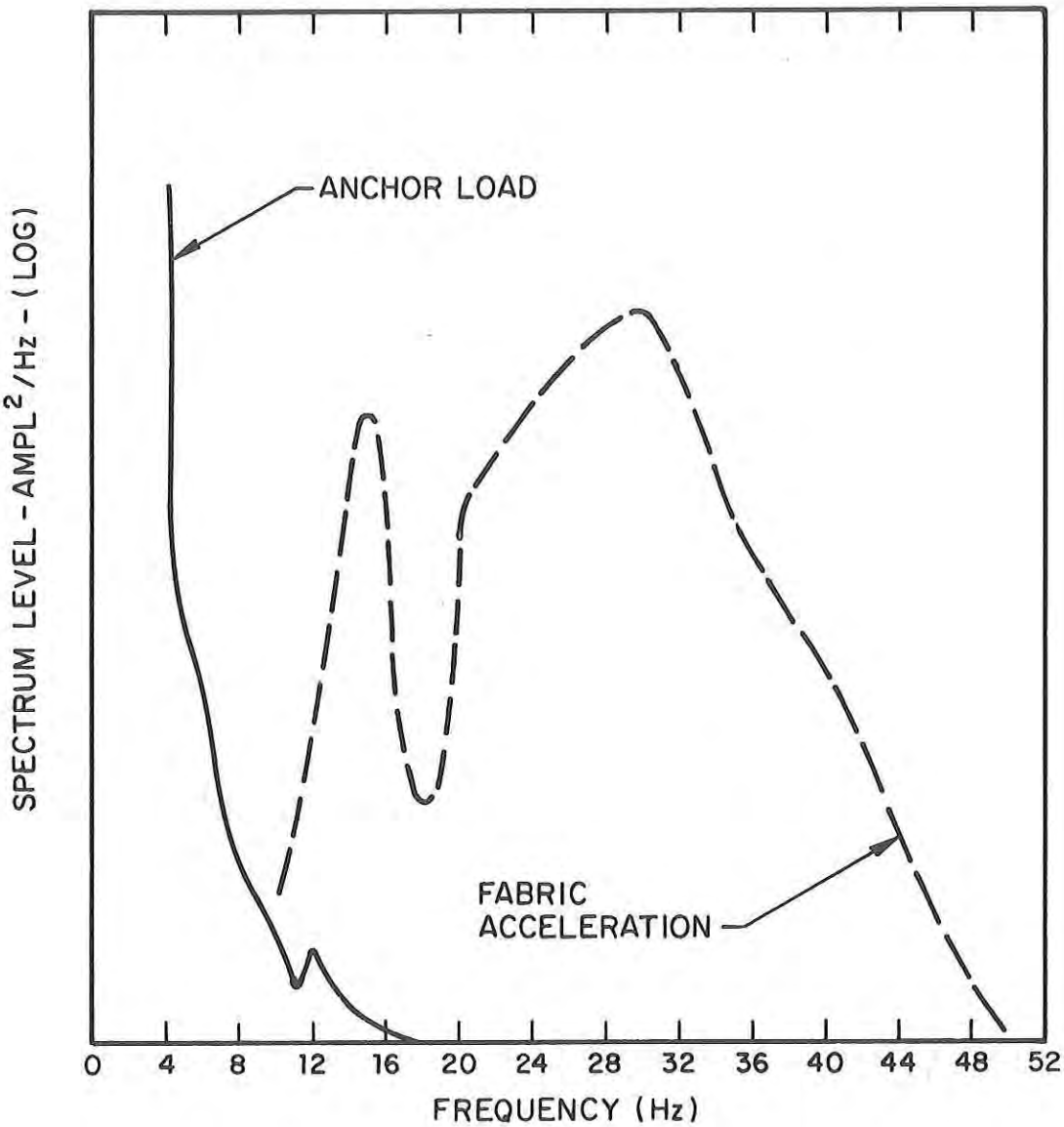

FIG. 18. COMPARISON OF THE ANCHOR LOAD AND FABRIC ACCELERATION SPECTRA FOR TEST 3.

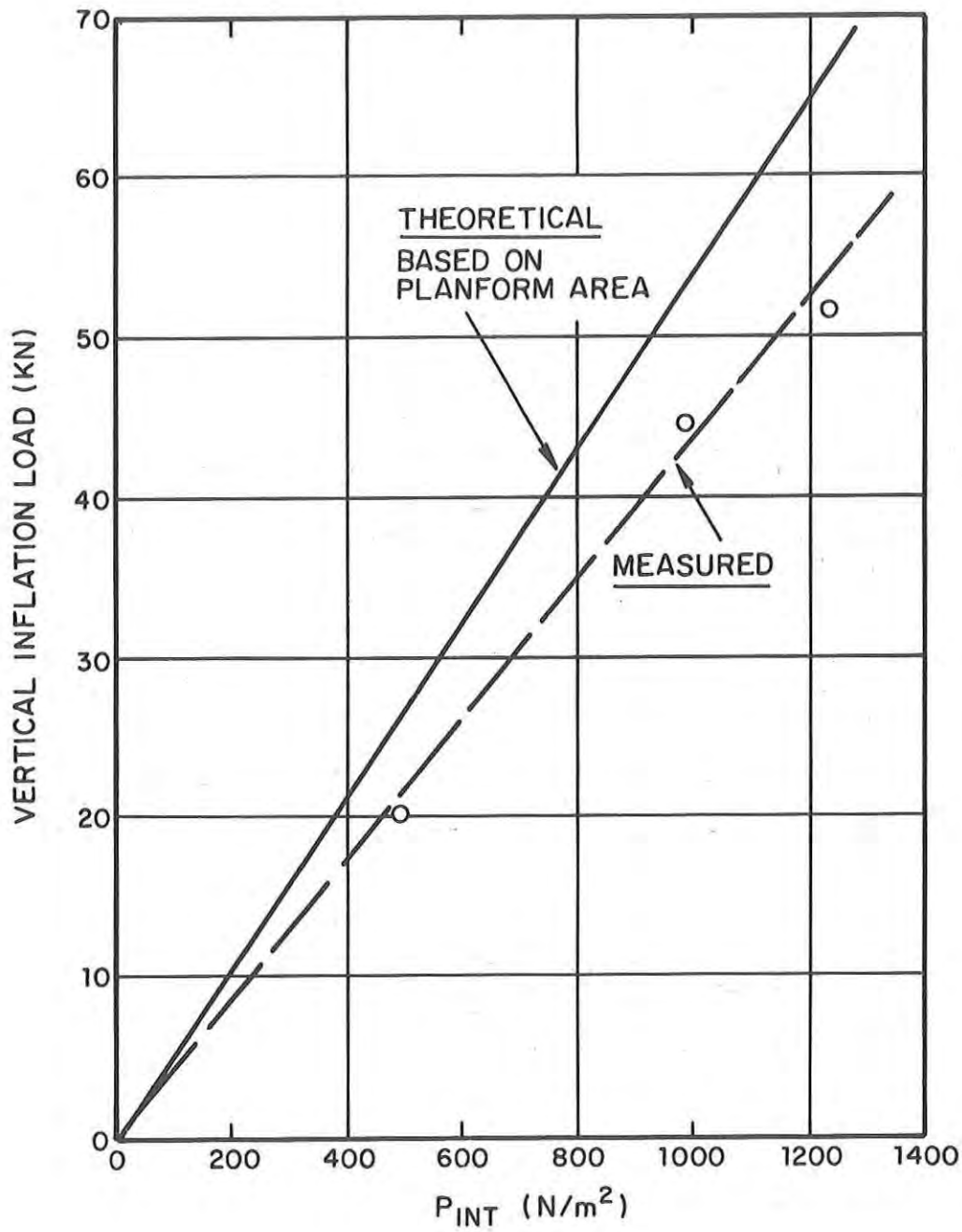

FIG. 19. VERTICAL INFLATION LOAD AS A FUNCTION OF INTERNAL PRESSURE.

estimate that the floor contact area is 42.8 m^2, i.e., 10.9 m^2 less than the planform area. Using a shelter circumference of 28.2 m, it is seen that the floor effectively leaves the ground plane over an equivalent annulus of 0.38 m, a finding that agrees with visual observation during the test.*

Since the internal pressure is of the same order of magnitude as the dynamic head during wind tunnel tests, it is clearly important to measure actual inflation loads, rather than calculate them from estimates of planform area, to prevent introducing significant errors into the test results. For design purposes, however, we recommend that the full planform area be used, since it is a conservative estimate.

It was also observed that the anchor loads varied widely around the circumference of the shelter. Figure 20 shows a typical variation of load with transducer position. The ordinate of the curve is inflation load normalized by mean inflation load, where mean inflation load is defined as inflation pressure times planform area divided by the number of tie-downs. Note that the load pattern can generally be explained by assigning a particular area to each transducer. The load is then the area times the inflation pressure. The scheme for dividing up the shelter planform area is shown in Fig. 21; the same distribution is shown, dotted, in Fig. 22. The dotted line (theoretical) is generally higher than the actual readings, since a fully active planform was used, rather than the reduced area explained above. Note the variations in loads seen by adjacent transducers; they are caused by individual rigging effects. However, the mean value over a group of transducers, such as 11 to 14, will be close to the theoretical value shown, modified by the reduced effective total area.

The use of this area subdivision, therefore, enables a good approximation of the individual anchor loads to be determined. It also points out that a design calculation that determines the average load will be in error by a factor of at least 1.4 when computing individual loads around a shelter

---

*Later, we will need to subtract out the contribution of the effective inflation pressure. To obtain the aerodynamic loads for this purpose, we will use the contact area of the shelter on the ground plane rather than the planform area. The contact area will be determined from Fig. 19.

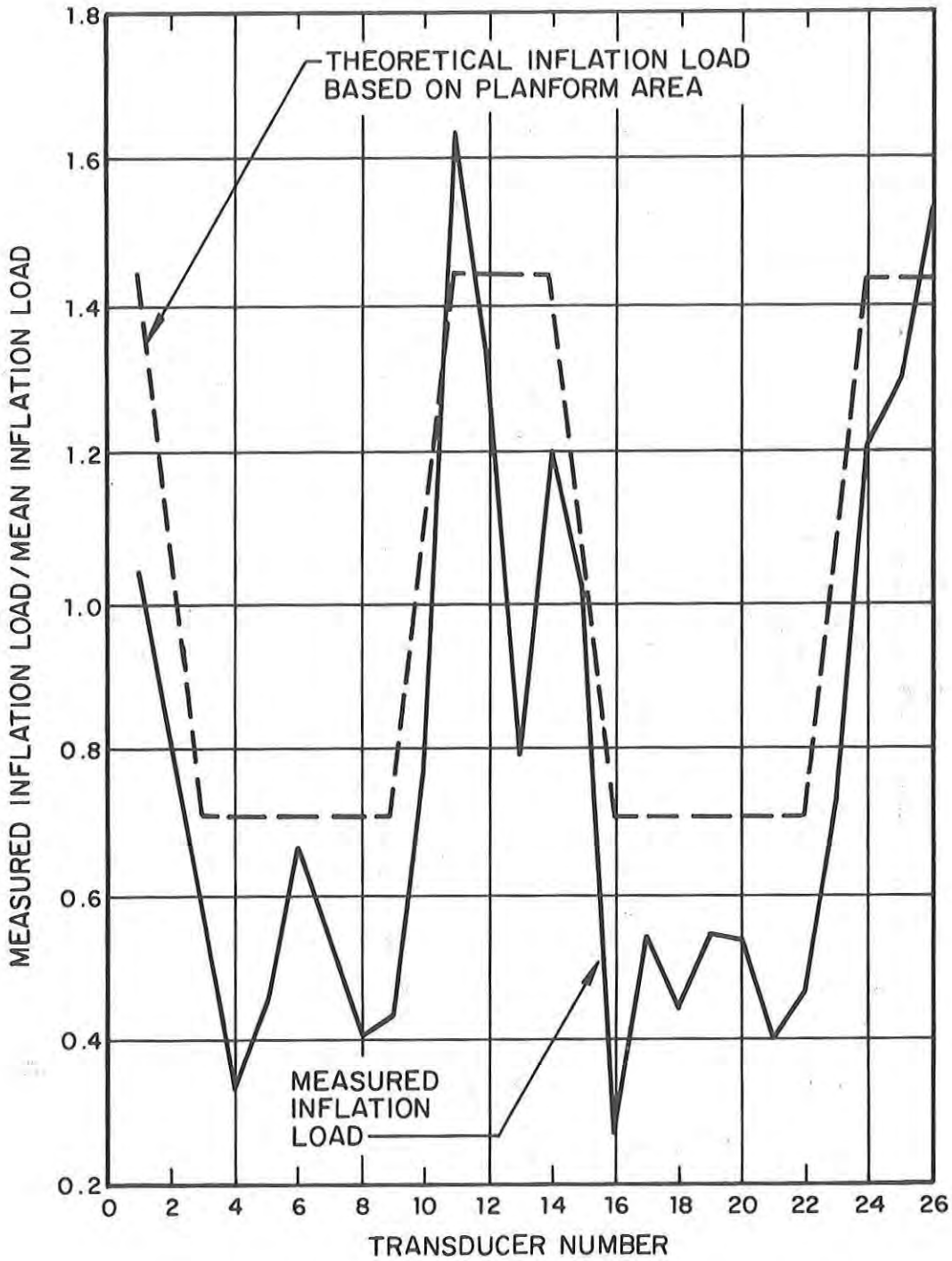

FIG. 20. INFLATION LOAD DISTRIBUTION.

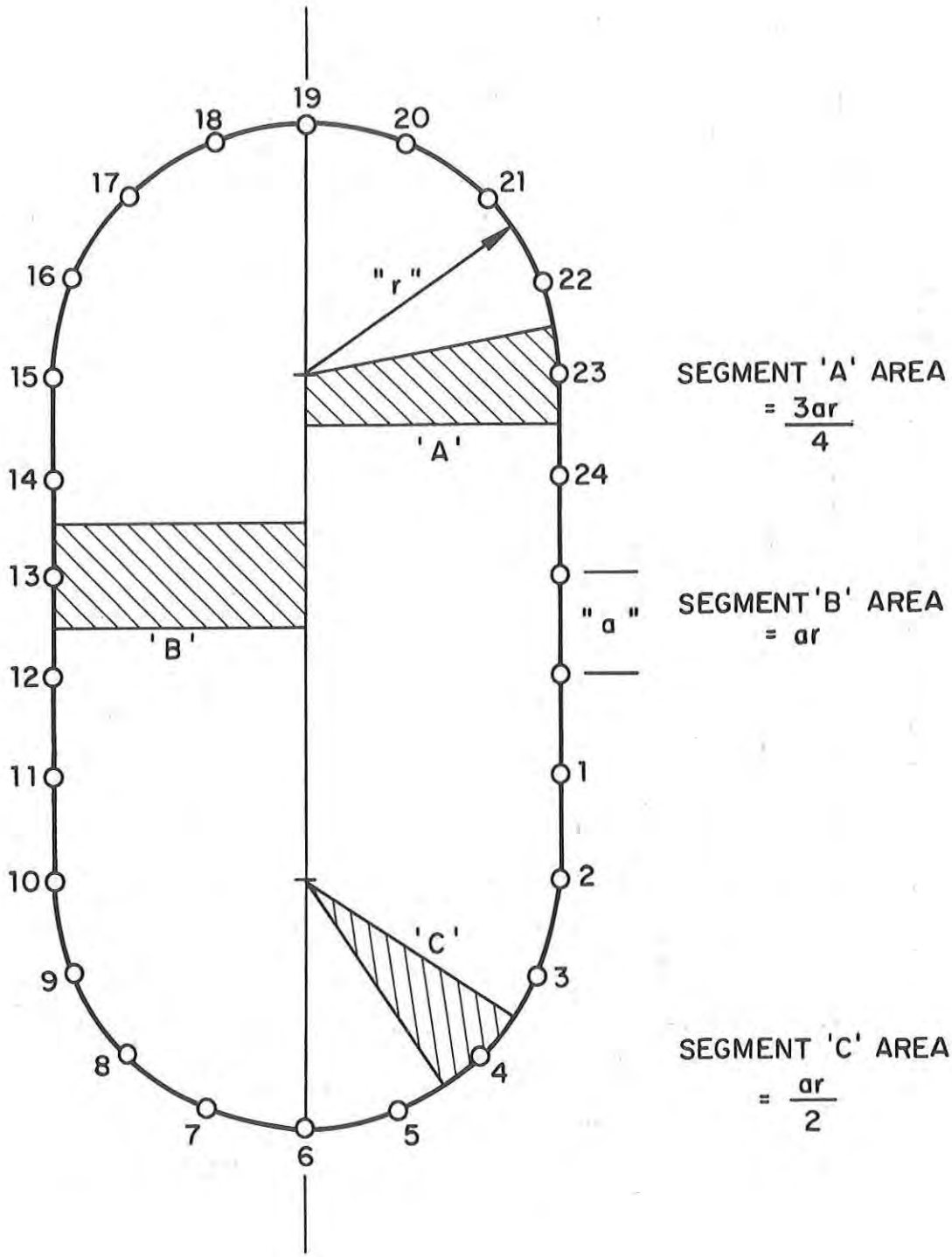

FIG. 21. PLANFORM AREA DISTRIBUTION FOR LOADING PROFILE.

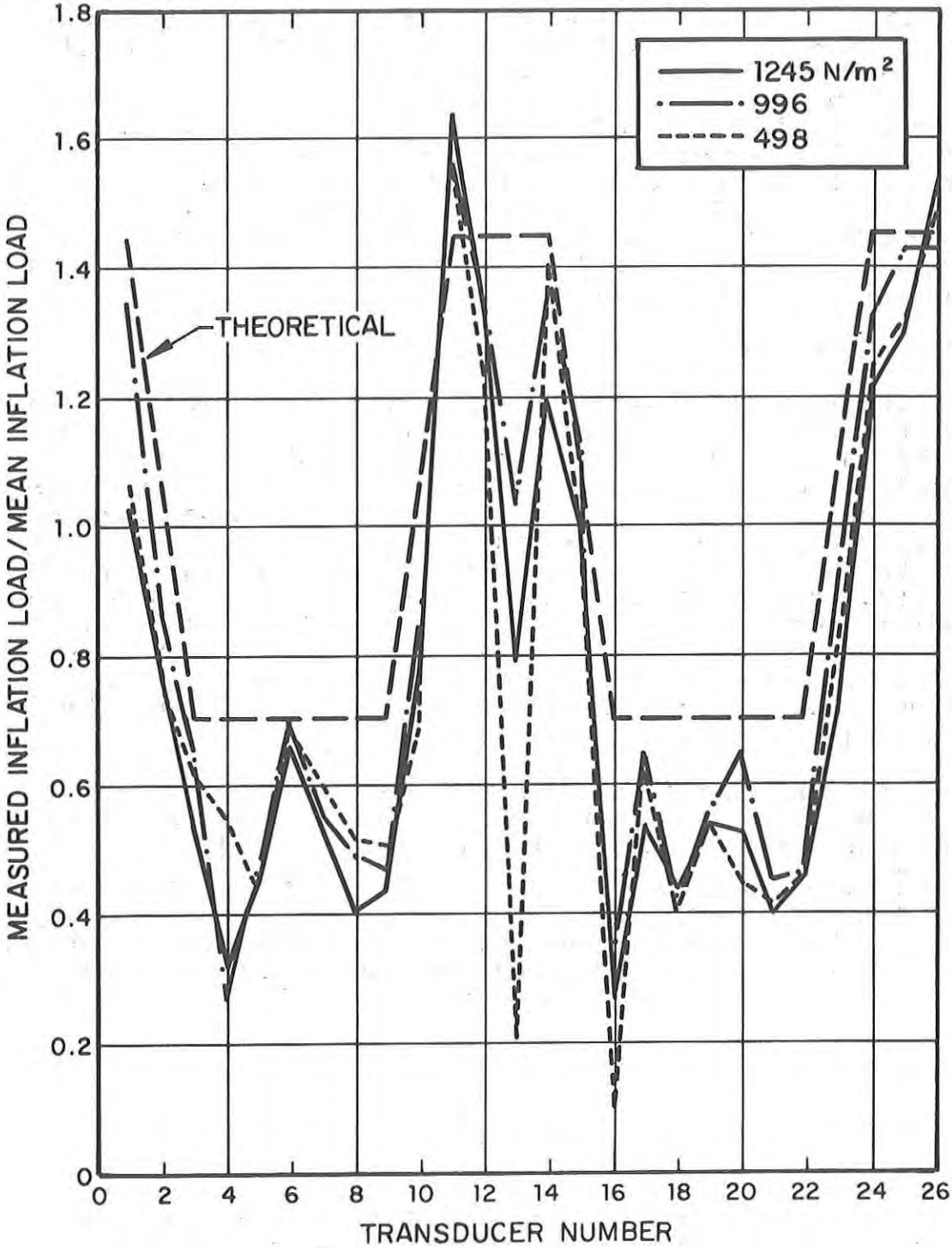

FIG. 22. SUMMARY OF INFLATION LOADS.

with equally spaced anchors. A more efficient use of anchors is one where each is arranged to carry an equal area segment rather than an equal circumferential length. Figure 22 illustrates the normalized inflation loads for all internal pressures tested and shows that essentially the pattern is quite consistent. Again, the theoretical estimate is somewhat above the mean of the measured results, since it is based upon the planform area. The marked drop-out of transducer 13 load at low inflation pressure is the result of a nonlinearity, probably due to a slack anchor line. The figure illustrates the effects of rigging of the shelter and indicates that tie-downs adjacent to a loose tie-down are quite effective in assuming its load. The problem of rigging and its ultimate affect on loads is clearly of interest and should be pursued in future programs.

5.2.2 Aerodynamic loads

The lift and drag coefficients for the single-wall shelter as a function of Reynolds number are presented in Fig. 23 for the 0 orientation. Since the Reynolds numbers are extremely high, both coefficients exhibit independence on Reynolds number. The lift coefficient appears to be reasonable; the drag coefficient is extremely low. Although it is not possible to ascertain why the drag coefficient is low, from the data we suspect that the reason is friction between the shelter floor and the ground plane. Previous tests, in which the ground plane was mounted to the wind tunnel balance rather than the wind tunnel floor, would give more realistic values of aerodynamic drag. However, they would not give more realistic estimates of tie-down loads.

The variation in aerodynamic load coefficients as a function of shelter orientation is given in Fig. 24. The C_x and C_y coefficients that form the drag coefficient are extremely low, as expected from Fig. 23. They are also somewhat independent of orientation, and, again, the reason appears to be friction between the floor and the ground plane. In order to obtain an estimate for the maximum decrease in the drag coefficient that may result from friction, we may write

$$\Delta C_{D_{max}} = \frac{\mu P_I}{q} \frac{A_T}{A_P} ,$$

where μ is the coefficient of friction between the shelter floor and the ground plane, and A_T is the area of the shelter

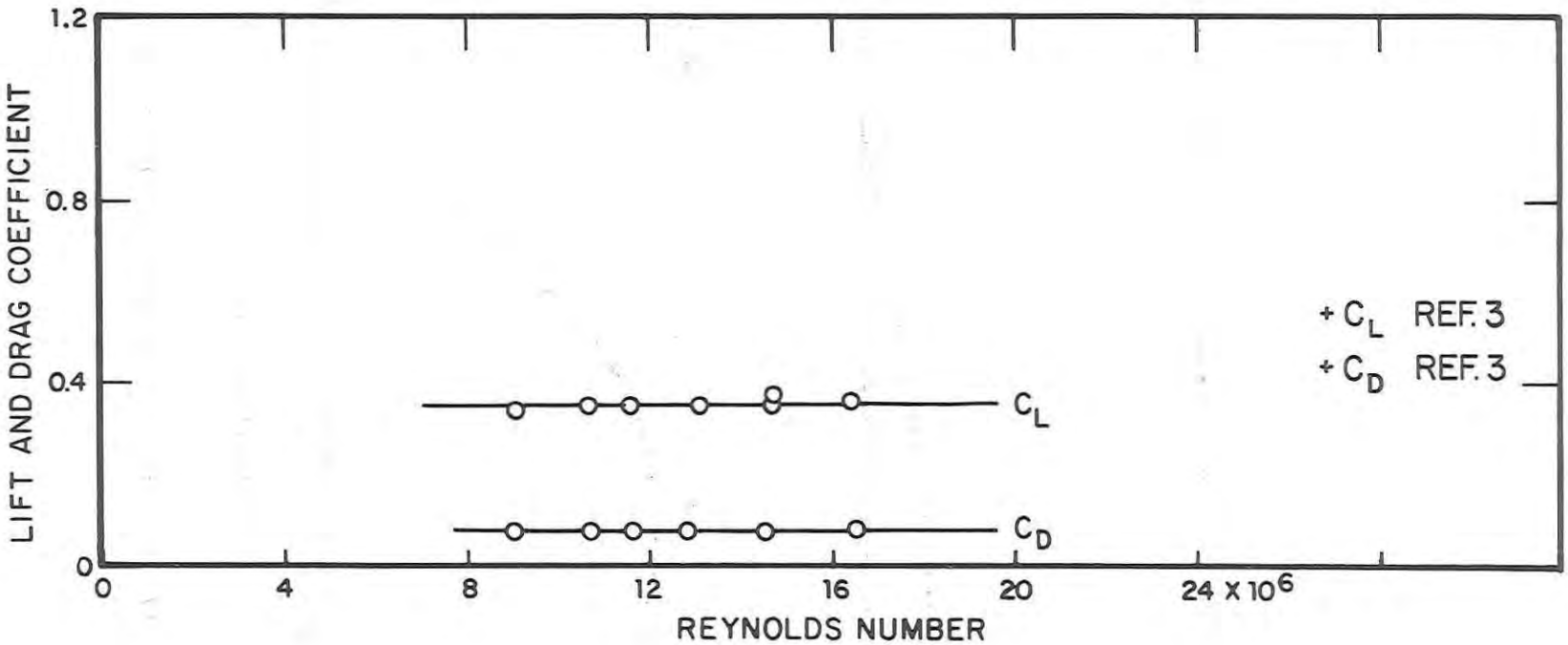

FIG. 23. LIFT AND DRAG COEFFICIENT AS A FUNCTION OF REYNOLDS NUMBER.

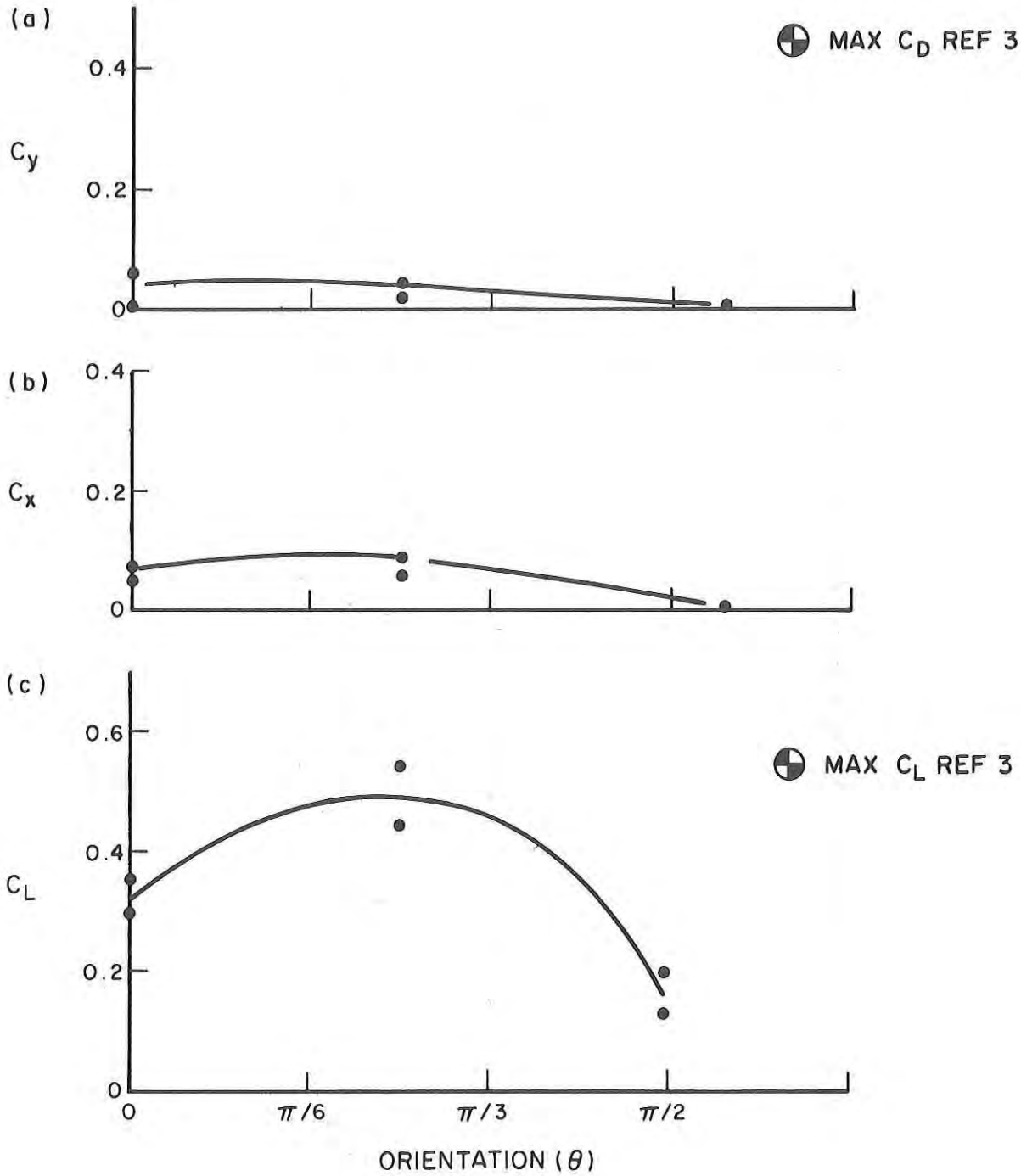

FIG. 24. SUMMARY OF FORCE COEFFICIENTS AS A FUNCTION OF ORIENTATION.

floor in contact with the ground plane. All other terms have been previously defined. The minimum value of P_I/q is 0.8 and, therefore,

$$\Delta C_{D_{max}} \approx .64\mu \ .$$

It is clearly possible that friction accounts for the low values of drag coefficient.

The magnitude of the lift coefficient is consistent with that measured in Ref. 1 and exhibits a dependence on orientation that is typical of previous results. The maximum overall anchor coefficient for the single-wall shelter at the $\pi/4$ orientation is plotted as a function of Reynolds number in Fig. 25. As in the case of the lift coefficient at the $\pi/4$ orientation, there is some scatter in the data. However, it would appear conservative to use a value of 0.75 as the overall anchor coefficient.

The distribution of anchor loads due to aerodynamic loading is plotted in Fig. 26 and compared to the inflation load distribution for a representative test. It is seen that the aerodynamic and inflation load distributions are virtually identical and that they both follow the distribution of area described above. The danger of averaging the calculated load around equally spaced anchors is clearly shown in Fig. 26. Without knowledge of the area effect, it would be assumed that all 26 anchors would carry 3.8% of the total load when, in fact, up to 8% may be carried on one anchor (#11).

5.2.3 Pressure distribution

Figure 27 presents the circumferential distribution of nondimensional pressure over the shelter surface at the 0 orientation. The data from all tests are summarized and bracketed by bars. The mean of the data is specified by a circle. The measured data is typical of that measured by taps away from the hemispherical ends of the shelter (i.e., 25 to 35, Fig. 6). Integration of the pressure distribution gives a lift coefficient in reasonable agreement with that presented earlier.

5.2.4 Spectra of tie-down loads and shelter accelerations

Spectral analysis of both the tie-down loads and the local shelter acceleration indicated that there was no

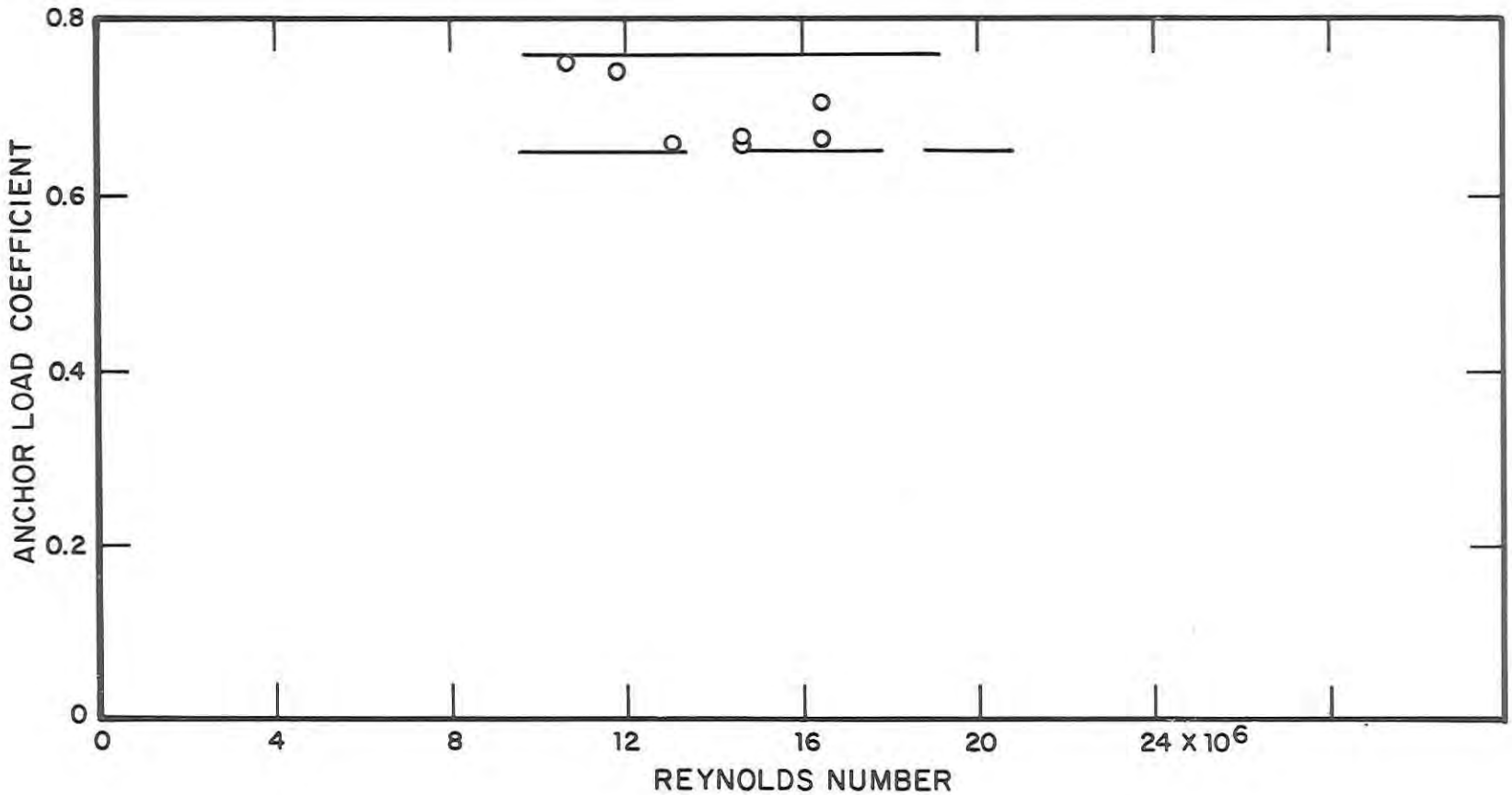

FIG. 25. SUMMARY OF ANCHOR COEFFICIENTS AS A FUNCTION OF REYNOLDS NUMBER FOR THE SINGLE-WALL SHELTER AT THE $\pi/4$ ORIENTATION.

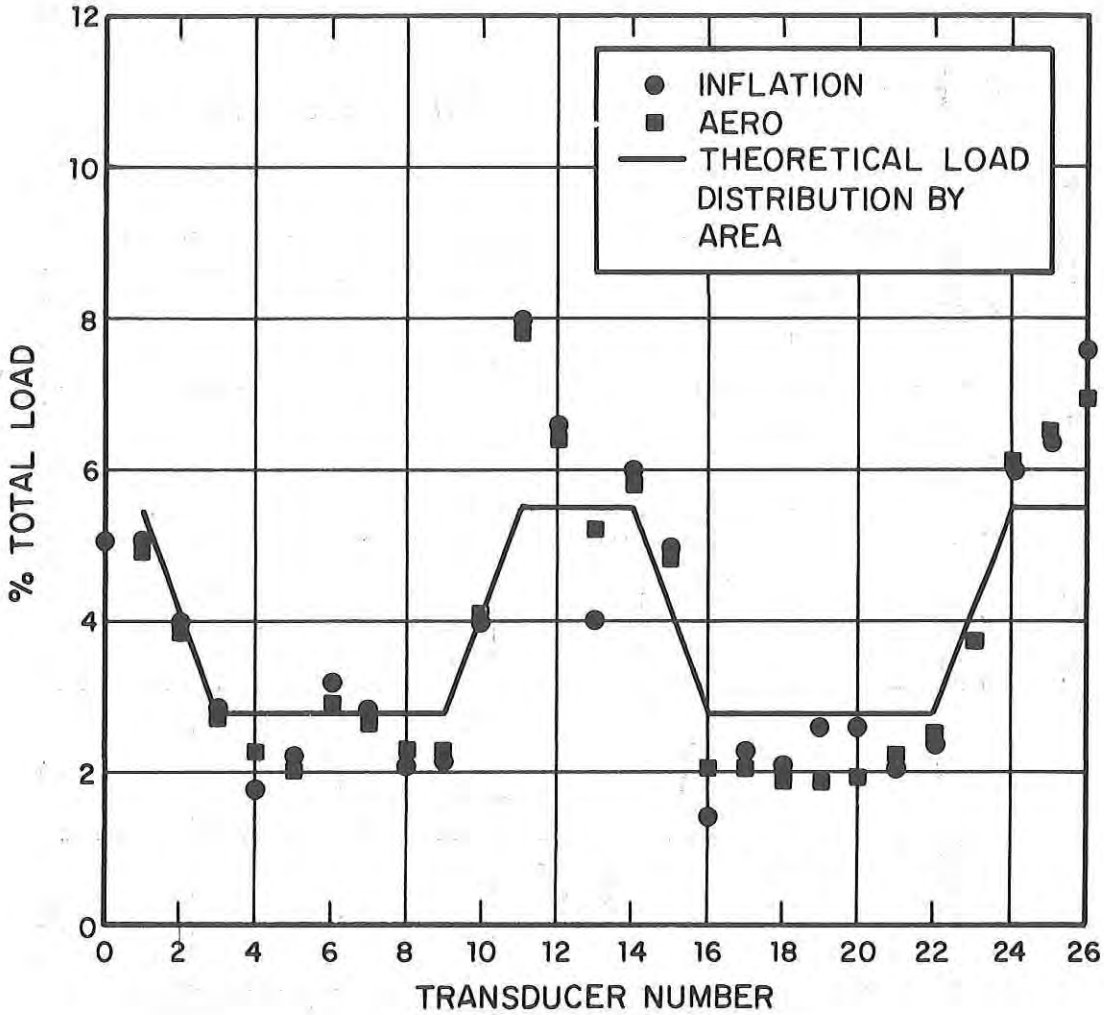

FIG. 26. AERODYNAMIC AND INFLATION LOAD DISTRIBUTION FOR THE SINGLE-WALL SHELTER AT THE $\pi/4$ ORIENTATION.

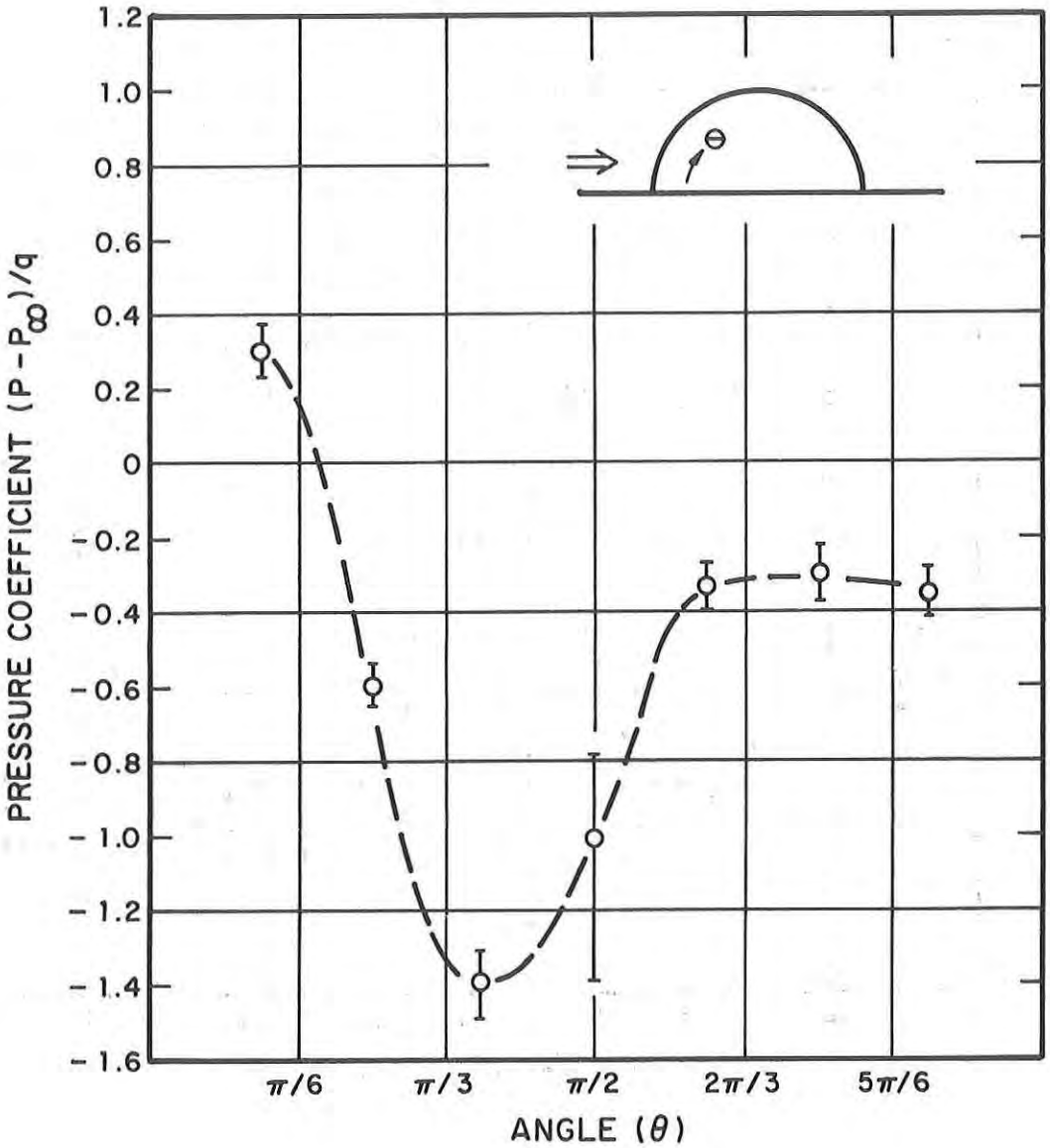

FIG. 27. PRESSURE DISTRIBUTION ON SINGLE-WALL SHELTER AS A FUNCTION OF ANGLE AT 0 ORIENTATION.

significant vibratory component in the measurements, and consequently we do not present a spectrum for either. This conclusion, although true for the range of internal pressures tested, may not be valid when the internal pressure is significantly less than the dynamic pressure of the air stream.

6. COMPARISON OF LARGE-SCALE SHELTER ANCHOR LOADS WITH EXTRAPOLATED RESULTS FROM SCALE MODELS

This section gives a numerical comparison of the tie-down loads predicted by Ref. 3 with those measured under the present program. It is important to recognize from the start that the load coefficients from Ref. 3 are defined on the basis of a maximum individual tie-down load times the number of tie-downs, whereas the coefficients in the present program are based upon a summation of the individual tie-down loads. Mathematically,

$$C_{\text{Ref. 3}} = \frac{nF_{max}}{qA}, \qquad C = \sum_{i=1}^{n} \frac{F_i}{qA},$$

where n is the number of tie-downs, F_{max} the maximum tie-down load, and the F_i are the individual tie-down loads.

6.1 Double-Wall Shelter

The anchor load and guyline load coefficients as given by Ref. 3 are 0.52 and 0.41, respectively. The maximum anchor and guyline loads at the highest Reynolds number are, therefore,

$$(\text{Anchor Load})_{\text{Ref. 3}} = \frac{C_{AL}qA}{n} = 2.31 \text{ kN},$$

$$(\text{Guyline Load})_{\text{Ref. 3}} = \frac{C_{GL}qA}{n} = 1.82 \text{ kN}.$$

Figure 15 gives the maximum anchor load and guyline loads as

$$\text{Anchor Load} = 0.097\ qA = 5.17 \text{ kN},$$

$$\text{Guyline Load} = 0.094\ qA = 5.03 \text{ kN}.$$

We note that both the anchor and guyline loads measured in the present program are larger by a factor of more than 2 than those predicted by Ref. 3. A comparison of the lift coefficients for both programs indicates that up to 60% of this difference may be due to differences between the tests (e.g., air stagnating under the shelter floor). However,

there still remains a considerable difference, which should be resolved by additional testing.

6.2 Single-Wall Shelter

The single-wall shelter loading is composed of both inflation loads and aerodynamic loads. Starting with the inflation load and an inflation pressure of 1245 N/m^2, Ref. 3 indicates that we should get

$$(\text{Inflation Load})_{\text{Ref. 3}} = \frac{P_I A_T}{n} = 2 \text{ kN} .$$

Reference to Fig. 22 gives a peak measured inflation load divided by mean inflation load of 1.65.

$$\text{Inflation Load} = 1.65 \frac{P_I A}{n} = 4.13 \text{ kN} .$$

Clearly, the measured results in the present program are appropriate for design usage, and the procedure defined in Ref. 3 should be modified.

The maximum aerodynamic load at the highest Reynolds number tested are now compared. The maximum anchor load coefficient of Ref. 3 is 1.36 and, therefore,

$$(\text{Anchor Load})_{\text{Ref. 3}} = \frac{C_{AL} qA}{n} = 4.38 \text{ kN} .$$

References to Figs. 25 and 26 give the anchor load coefficient as 0.75 and the maximum percent of the total load carried by an individual anchor as 8%.

$$\text{Inflation Load} = 0.08\ C_{AL} qA = 5 \text{ kN} .$$

These loads are in reasonable agreement, and differences are no doubt due to rigging differences between the shelters.

Summarizing the comparison:

- Predicted anchor loads for the double-wall shelter are a factor of 2 less than measured anchor loads.

Additional testing should be conducted to resolve the discrepancy.

- Predicted inflation loads for the single-wall shelters are a factor of 2 less than measured loads. A change in the prediction procedure is therefore warranted.

- Predicted aerodynamic loading for the single-wall shelter is in relatively good agreement with measured values.

REFERENCES

1. Dietz, A.E., Proffitt, R.B., and Chabot, R.S., "Wind Tunnel Tests and Analyses of Ground Mounted Air-Supported Structures," U.S. Army Natick Laboratories, Technical Report No. 67-36-ME (AD 65 1954), October 1966.

2. MIT Department of Aeronautics and Astronautics, "Wind Tunnel Tests on an Air Supported Tent Model," Report No. 1024, June 1963.

3. Dietz, A.E., Proffitt, R.B., Chabot, R.S., and Moak, E.L., "Design Manual for Ground Mounted Air-Supported Structures (Single and Double Wall)," revised. U.S. Army Natick Laboratories, Technical Report 69-59-GP, January 1969.

4. Clemente, A.R., Madden, R., Blackwell, J.B., and Remington, P.J., "Three Directional Load Transducer," U.S. Army Natick Laboratories, Technical Report 74-28-GP (AD 776356), April 1973.

5. Chien, N. et al., "Wind Tunnel Studies of Pressure Distribution on Elementary Building Forms," Iowa Institute of Hydraulic Research, Iowa State University, 1951.

LIST OF SYMBOLS

A	area
A_p	planform area
A_T	area of shelter in contact with ground plane
C_{AL}	anchor load coefficient, (anchor load)/qA
C_D	drag coefficient, (drag force)/qA
C_{GL}	guyline load coefficient, (guyline load)/qA
C_L	lift coefficient, (lift force)/qA
C_P	pressure coefficient, $(P-P_\infty)/q$
C_x	x-force coefficient
c_y	y-force coefficient
D	shelter diameter
F	force
n	number of tie-downs
N_R	Reynolds number
P	pressure
P_I	inflation pressure
P_{IE}	effective inflation pressure
P_∞	ambient pressure
q	dynamic pressure, $1/2\rho V_\infty^2$
V	velocity
V_∞	freestream velocity
x	Cartesian coordinate
y	Cartesian coordinate
θ	angle

μ	coefficient of friction
ν	kinematic viscosity
ρ	density